This is a repository copy of *Hawking Radiation from Higher-Dimensional Black Holes*.

Hawking radiation from higher-dimensional black holes

Panagiota Kanti[1] and Elizabeth Winstanley[2]

[1] Division of Theoretical Physics, Department of Physics, University of Ioannina,
Ioannina. GR-451 10 Greece
`pkanti@cc.uoi.gr`
[2] Consortium for Fundamental Physics, School of Mathematics and Statistics,
The University of Sheffield, Hicks Building, Hounsfield Road, Sheffield. S3 7RH
United Kingdom
`e.winstanley@sheffield.ac.uk`

Summary. We review the quantum field theory description of Hawking radiation from evaporating black holes and summarize what is known about Hawking radiation from black holes in more than four space-time dimensions. In the context of the Large Extra Dimensions scenario, we present the theoretical formalism for all types of emitted fields and a selection of results on the radiation spectra. A detailed analysis of the Hawking fluxes in this case is essential for modelling the evaporation of higher-dimensional black holes at the LHC, whose creation is predicted by low-energy models of quantum gravity. We discuss the status of the quest for black-hole solutions in the context of the Randall-Sundrum brane-world model and, in the absence of an exact metric, we review what is known about Hawking radiation from such black holes.

1 Introduction

Hawking radiation [1] is one of the most important effects arising from quantum field theory in curved space, a semi-classical approach to quantum gravity. In this framework space-time is described by a classical geometry, governed by the Einstein equations (or an alternative classical theory of gravity). The behaviour and propagation of quantum fields on a fixed (but not necessarily stationary) space-time is then studied. Hawking radiation is thermal in nature, giving non-extremal black holes an intrinsic temperature proportional to the surface gravity of the event horizon. For a Schwarzschild black hole in asymptotically flat space, the specific heat is negative, so that the temperature increases as the black hole evaporates, leading to a black hole explosion. The ultimate fate of the black hole depends on unknown details of quantum gravity, but black hole evaporation raises many deep questions about the nature of quantum gravity and the fundamental laws of physics (such as the information loss paradox, see, for example, [2, 3]). Here we will not address

these important issues, but instead focus on the detailed properties of the Hawking radiation itself.

Hawking radiation from four-dimensional black holes in asymptotically flat space was studied in detail by Page [4, 5, 6]. Over the past fifteen or so years, there has been great interest in higher-dimensional black holes. Within the context of classical general relativity, a menagerie of black-hole-like solutions of the Einstein equations has been discovered (see for example [7, 8] for reviews). It is then natural to study the properties of Hawking radiation from higher-dimensional black holes.

This avenue of research gained much impetus from the exciting possibility of producing microscopic higher-dimensional black holes in high-energy collisions either at the LHC or in cosmic rays [9, 10, 11, 12, 13, 14, 15, 16]. This is a prediction of higher-dimensional brane-world models [17, 18, 19, 20, 21] in which the energy scale of quantum gravity is much lower than the traditional value of 10^{19} GeV, and may be as low as the TeV-scale. If such a microscopic black hole is produced, it will initially be rapidly rotating and rather asymmetric. Its subsequent evolution can be modelled as four stages [11]:

- During the *balding phase* the black hole sheds its asymmetries through the emission of gravitational radiation and also loses any gauge field charges arising from the particles which formed it. At the end of this stage the black hole is axisymmetric and still rapidly rotating.
- The black hole then emits Hawking radiation, and loses both mass and angular momentum. At the end of this *spin-down phase* the black hole is no longer rotating.
- Now with zero angular momentum, the black hole continues to radiate during the *Schwarzschild phase*, shrinking as it loses mass.
- During the final *Planck phase* the semi-classical approximation for the Hawking radiation is no longer valid and the black hole emission depends on the details of quantum gravity.

It is expected that the spin-down and Schwarzschild phases will dominate the lifetime of the black hole. A detailed understanding of the Hawking radiation from higher-dimensional black holes in brane-world models is therefore necessary for simulating microscopic black hole events [22, 23] and experimental searches, as well as being of intrinsic theoretical interest.

In this chapter we focus on the theoretical modelling of Hawking radiation from higher-dimensional black holes. We begin with a discussion of the quantum-field-theoretic derivation of Hawking radiation and its description using the Unruh vacuum state [24]. We then briefly review some key features of black holes in brane world models. We describe the formalism for studying quantum fields on higher-dimensional Myers-Perry black holes [25], which model black holes in an ADD brane-world [17, 18, 19]. We also present a selection of results on the properties of the Hawking radiation from these black holes. The literature on this subject is vast and so we cannot claim to do all aspects justice. The reviews [12, 26, 27, 28, 29] contain further discussion of results which space does not permit us to include. In the RS brane-world [20, 21], analysis of the Hawking radiation is more challenging because no exact metric describing a five-dimensional black hole localised on the brane is known in general - for a more detailed discussion of this topic, see the reviews [30, 31, 32]. We close the chapter with a discussion of what is known about the Hawking radiation in this case.

2 Hawking radiation

2.1 Hawking radiation from a black hole formed by gravitational collapse

Hawking's original derivation [1] considered a quantum scalar field propagating on a fixed, but dynamic, background space-time corresponding to the formation of a four-dimensional Schwarzschild black hole by the gravitational collapse of matter in asymptotically flat space. The Penrose diagram for this process is shown in Figure 1 (cf. the Penrose diagram for an eternal Schwarzschild black hole in Figure 2).
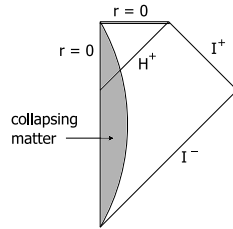
Fig. 1. Penrose diagram for a Schwarzschild black hole formed by gravitational collapse.
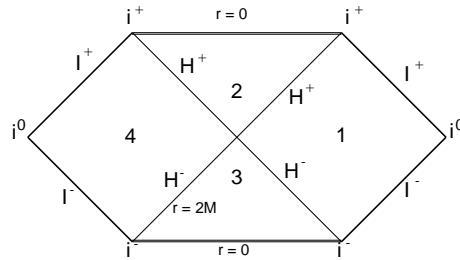
Fig. 2. Penrose diagram for an eternal Schwarzschild black hole

For the moment consider a massless scalar field in a two-dimensional version of the space-time shown in Figure 1, with space-time co-ordinates (t, r). In this case, because two-dimensional space-times are locally conformally flat, a basis of field modes is formed simply from plane waves. These plane waves are not normalizable, but normalizable wave-packets can be constructed from appropriate linear combinations of the plane wave modes. At very early times, long before the collapse starts, a suitable basis of field modes is:

$$\phi_\omega \propto e^{-i\omega t} e^{\pm i\omega r}, \tag{1}$$

where $\omega > 0$ corresponds to positive frequency. The quantum scalar field $\hat{\Phi}$ is written in terms of these basis modes:

$$\hat{\Phi} = \int_{\omega=0}^{\infty} d\omega \left[\hat{a}_\omega \phi_\omega + \hat{a}_\omega^\dagger \phi_\omega^* \right], \tag{2}$$

where the expansion coefficients a_ω have been promoted to operators in the canonical quantization of the scalar field. Working in the Heisenberg picture, the quantum state is defined to be the "in" vacuum at early times near I^-, namely the state $|0\rangle_{\text{in}}$ which is annihilated by the $\hat{a}_\omega$ operators:

$$\hat{a}_\omega |0\rangle_{\text{in}} = 0 \qquad \forall \omega > 0. \tag{3}$$

At late times, long after the black hole has formed, we can form a basis of field modes similar to (1), write the quantum scalar field in terms of these modes along the lines of (2) but with the expansion coefficients $\hat{a}_\omega$ now replaced by operators $\hat{b}_\omega$, and define an "out" vacuum state $|0\rangle_{\text{out}}$ which is annihilated by the $\hat{b}_\omega$ operators.

The crux of Hawking's derivation [1] is that the "in" and "out" vacuum states are not the same: the "in" vacuum $|0\rangle_{\text{in}}$ contains a thermal flux of outgoing particles at late times near I^+ (we use units in which $c = \hbar = G = k_B = 1$):

$$_{\text{in}} \left\langle 0 \left| \hat{b}_\omega^\dagger \hat{b}_\omega \right| 0 \right\rangle_{\text{in}} = \frac{1}{e^{\omega/T_H} - 1} \tag{4}$$

where

$$T_H = \frac{\kappa}{2\pi} \tag{5}$$

is the Hawking temperature and κ is the surface gravity of the black hole. There are many different derivations of this effect (see, for example, [33, 34, 35, 36, 37, 38, 39, 40, 41, 42, 43, 44]). Hawking's result is very robust, and essentially kinematic: it is independent of the Einstein equations or the theory of gravity under consideration. There are a number of different pictures to understand the origin of the thermal flux, such as quantum tunnelling of classically forbidden trajectories from behind the event horizon [40], or the pair creation of quantum particles close to the event horizon, one of which carries negative energy down the event horizon and the other of which escapes to infinity. In terms of modes, the thermal factor arises because outgoing modes at I^+ can be traced back to ingoing modes which enter the collapsing body just before the last ingoing mode (which then forms the event horizon of the black hole after reflection from the co-ordinate centre $r = 0$), resulting in a "pile-up" of highly blue-shifted modes near this last ingoing mode.

Using a geometric optics argument, Hawking's result can be extended to black holes in four or more space-time dimensions [1]. The complication is that, even for a massless scalar field, in more than two space-time dimensions the quantum field interacts with a gravitational potential which surrounds the black hole. As a result, a wave which is outgoing near the event horizon of the black hole will partly escape to infinity and partly be reflected back down the event horizon. The part which escapes to I^+ will contribute to the Hawking flux. In four or more space-time dimensions, each mode of a quantum field of spin s will be characterized by its frequency ω, a total angular momentum quantum number ℓ, an azimuthal quantum number m

(indexing the angular momentum about the z-axis) and, in more than four space-time dimensions, further angular quantum numbers j. To describe this scattering effect we introduce the grey-body factor $\Gamma_{s\omega\ell mj}$ which is given by the outgoing flux near I^+ for each mode divided by the outgoing flux near the horizon in that mode (that is, the fraction of each outgoing mode near the horizon which is transmitted to I^+). The Hawking flux (4) is then modified to be, for each quantum field mode:

$$\text{in} \left\langle 0 \left| \hat{b}_\omega^\dagger \hat{b}_\omega \right| 0 \right\rangle_\text{in} = \frac{\Gamma_{s\omega\ell mj}}{e^{\omega/T_H} \pm 1}, \tag{6}$$

where the $+$ sign in the denominator is for fermionic fields and the $-$ sign for bosonic fields. While Hawking's original derivation [1] was for a quantum scalar field, we emphasize that the result carries over to quantum fields of all spins. Furthermore, although in the above we have considered a Schwarzschild black hole, any black hole with a non-extremal event horizon will emit Hawking radiation, including rotating black holes. In this article we will consider only rotating black holes with a single axis of rotation (which we take to be the z-axis). In this case the denominator of the Hawking flux (6) is modified by the rotation of the black hole to be

$$e^{\tilde{\omega}/T} \pm 1 \tag{7}$$

where

$$\tilde{\omega} = \omega - m\Omega_H, \tag{8}$$

with m the azimuthal quantum number and Ω_H is the angular velocity of the event horizon.

2.2 The Unruh state

In practice, dealing with quantum fields on the dynamical space-time shown in Figure 1 is technically difficult. In computing Hawking radiation, a different approach is usually employed. Instead of considering the collapse geometry of Figure 1, the eternal black hole space-time (such as that for the Schwarzschild black hole shown in Figure 2) is considered. We restrict our attention to the right-hand-diamond of Figure 2, representing the region exterior to the black hole event horizon. Charged and/or rotating black holes have more complex Penrose diagrams than Figure 2, but the diamond-shaped region exterior to the event horizon is the same for all asymptotically-flat black holes. For black holes in de Sitter space, the relevant region is that between the event and cosmological horizons, which has the same diamond shape.

The Unruh state [24] is the quantum state on the eternal black hole space-time which models the Hawking radiation. The construction of this state proceeds as follows, where for simplicity we consider a free massless scalar field Φ and a four-dimensional Schwarzschild black hole with co-ordinates (t, r, θ, φ). In this case the scalar field modes $\phi_{\omega\ell m}$ are separable:

$$\phi_{\omega\ell m}(t, r, \theta, \varphi) = e^{-i\omega t} e^{im\varphi} R_{\omega\ell m}(r) Y_{\ell m}(\theta), \tag{9}$$

where ω is the frequency of the mode, m is the azimuthal quantum number, ℓ is the total-angular-momentum quantum number, $R_{\omega\ell m}(r)$ is the radial function and $Y_{\ell m}(\theta)$ is a spherical harmonic. First a basis of quantum field modes is required.
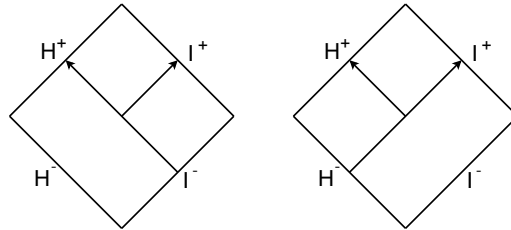
Fig. 3. "In" (left) and "up" (right) modes

We take as a basis the "in" and "up" modes depicted in Figure 3. The "in" modes $\phi_{\omega\ell m}^{\mathrm{in}}$ are incoming from past null infinity I^-. Part of each wave is reflected by the gravitational potential and scatters back to infinity, and part goes down the future event horizon H^+. The "up" modes $\phi_{\omega\ell m}^{\mathrm{up}}$ are outgoing from close to the past event horizon H^-. In this case part of each wave is reflected back down the future event horizon H^+, while part is transmitted to future null infinity I^+.

Having chosen a suitable basis of field modes, we now need to split these modes into positive and negative frequency. For the "in" modes, we choose 'positive frequency' to mean 'positive frequency as seen by a static observer far from the black hole', so that, for a field mode $\phi_{\omega\ell m}$ we have:

$$\frac{\partial}{\partial t}\phi_{\omega\ell m} = -i\omega\phi_{\omega\ell m}, \tag{10}$$

where $\omega > 0$. Since the "in" modes originate from near I^-, this is the most natural choice of positive frequency for these modes. For the "up" modes, we choose 'positive frequency' to mean 'positive frequency with respect to Kruskal time near the event horizon'. Since the "up" modes originate from near H^-, this choice of positive frequency, with respect to co-ordinates which are regular across the event horizon, is also very natural. We decompose our quantum field $\hat{\Phi}$ in terms of this basis of positive frequency modes:

$$\hat{\Phi} = \sum_{\mathrm{modes}} \left[\hat{a}_{\omega\ell m}^{\mathrm{in}}\phi_{\omega\ell m}^{\mathrm{in}} + \hat{a}_{\omega\ell m}^{\mathrm{in}\dagger}\phi_{\omega\ell m}^{\mathrm{in}*}\right] + \sum_{\mathrm{modes}} \left[\hat{a}_{\omega\ell m}^{\mathrm{up}}\phi_{\omega\ell m}^{\mathrm{up}} + \hat{a}_{\omega\ell m}^{\mathrm{up}\dagger}\phi_{\omega\ell m}^{\mathrm{up}*}\right] \tag{11}$$

where in each case the sum is taken over the positive frequency modes and we have promoted the expansion coefficients for the classical scalar field to operators satisfying the usual commutation relations:

$$\left[\hat{a}_{\omega\ell m}^{\mathrm{in/up}}, \hat{a}_{\omega'\ell'm'}^{\mathrm{in/up}\dagger}\right] = \delta(\omega-\omega')\delta_{\ell,\ell'}\delta_{m,m'}, \quad \left[\hat{a}_{\omega\ell m}^{\mathrm{in/up}}, \hat{a}_{\omega'\ell'm'}^{\mathrm{in/up}}\right] = 0 = \left[\hat{a}_{\omega\ell m}^{\mathrm{in/up}\dagger}, \hat{a}_{\omega'\ell'm'}^{\mathrm{in/up}\dagger}\right]. \tag{12}$$

The Unruh state $|U\rangle$ [24] is then defined as that state which is annihilated by the operators $\hat{a}_{\omega\ell m}^{\mathrm{in/up}}$:

$$\hat{a}_{\omega\ell m}^{\mathrm{in/up}}|U\rangle = 0. \tag{13}$$

This state has no particles in the "in" modes near I^- as was the case for the "in" vacuum $|0\rangle_{\mathrm{in}}$ describing the state for a black hole formed by gravitational collapse. However, due to the choice of positive frequency for the "up" modes, these modes are

thermally populated with temperature T_H (5). Therefore, near future null infinity I^+, a static observer will see an outgoing flux of particles in the "up" modes, which is precisely the Hawking radiation. Furthermore, the flux in each mode will be given by (6), with the grey-body factor $\Gamma_{\omega\ell m}$ (with spin $s = 0$ and no index j because we are in four space-time dimensions) representing the proportion of each "up" mode which escapes to I^+.

Here we have discussed the construction of the Unruh state for the particular example of a massless scalar field on a four-dimensional Schwarzschild space-time. The extension of this construction to higher-dimensional, spherically-symmetric space-times is straightforward. For higher-spin fields, the field modes are more complicated than (9) but the construction works in a similar way (bearing in mind that the Hawking flux (6) has a $+$ sign in the denominator for fermion fields and a $-$ sign for bosonic fields). The Unruh state can also be constructed for rotating black holes. In this case the frequency ω in the thermal factor in (6) becomes $\tilde{\omega}$ (8). This shift arises because $\tilde{\omega}$ rather than ω is the natural frequency of field modes near the horizon of a rotating black hole, from where the Hawking radiation emanates. For details of this construction on four-dimensional Kerr black holes, see [45] (scalars), [46] (fermions) and [47] (electromagnetism).

In order to compute the fluxes of particles, energy and angular momentum emitted in Hawking radiation we calculate expectation values of the appropriate operators in the Unruh state on an eternal black hole space-time. The flux of particles per unit time is given by summing the individual mode flux (6) over all field modes:

$$\frac{dN}{dt} = \sum_{\text{modes}} \frac{\Gamma_{s\omega\ell m j}}{e^{\tilde{\omega}/T_H} \pm 1},$$
(14)

where the exact form of the sum over the modes will be made precise in section 4, and $\tilde{\omega} = \omega$ if the black hole is non-rotating. The fluxes of energy and (for a rotating black hole) angular momentum per unit time are given by expectation values of the quantum stress-energy tensor for the particular quantum field under consideration:

$$\frac{dE}{dt} = \int r^2 \, d\Omega \, \langle U \, | \hat{T}^r_t | \, U \rangle, \qquad \frac{dJ}{dt} = \int r^2 \, d\Omega \, \langle U \, | \hat{T}^{r\varphi} | \, U \rangle,$$
(15)

where the integral is taken over the sphere at infinity and we have given the expressions for four-dimensional black holes.

Expectation values of the stress-energy tensor typically require renormalization, due to their involving products of two operators at the same space-time point. One method of renormalization is covariant geodesic point separation, in which the two operators whose products are taken are evaluated at different space-time points x and x', yielding a finite bitensor stress-energy tensor, whose expectation value is written $T_{\mu\nu}(x, x')$. This expectation value is renormalized by the subtraction of purely geometric, state independent renormalization terms $T_{\mu\nu}^{\text{div}}(x, x')$ (see for example [48, 49] for expressions for these geometric terms for fields of spin 0, 1/2 and 1 in four dimensions, and [50] for a scalar field in higher-dimensional space-time). The points x and x' are then brought together and a finite renormalized expectation value for the stress-energy tensor is yielded.

Fortunately, for the black holes in which we are interested, it can be shown that the two stress-energy tensor components in (15) do not require renormalization. For a quantum scalar field on a four-dimensional Kerr black hole, this was

shown by Frolov and Thorne [51]. Their argument involved two key properties: (i) the symmetry of the underlying space-time under the reflection $(t, \varphi) \rightarrow (-t, -\varphi)$ (simultaneous reversal of time and the azimuthal angle); and (ii) each of the geometric subtraction terms involves an even number of covariant derivatives σ^{μ} of the biscalar of geodetic interval [52] when an average has been taken over a separation in the σ^{μ} and $-\sigma^{\mu}$ directions. Choosing radial point-splitting, these two properties ensure that the geometric subtraction terms $T_{tr}^{\mathrm{div}}(x, x')$ and $T_{r\varphi}^{\mathrm{div}}(x, x')$ both vanish. Since the two properties above are shared by the simply-rotating black holes which we shall consider in section 4, the above argument can be readily extended to show that $T_{tr}^{\mathrm{div}}(x, x')$ and $T_{r\varphi}^{\mathrm{div}}(x, x')$ both vanish for these black holes as well [53].

The exact form of the stress-energy tensor components in (15) depends on the spin of the quantum field under consideration (see, for example, [12, 53, 54, 55, 56] for details). However, the resulting fluxes of energy and angular momentum have the following simple forms:

$$\frac{dE}{dt} = \sum_{\text{modes}} \frac{\omega \Gamma_{s\omega\ell mj}}{e^{\tilde{\omega}/T_H} \pm 1}, \qquad \frac{dJ}{dt} = \sum_{\text{modes}} \frac{m \Gamma_{s\omega\ell mj}}{e^{\tilde{\omega}/T_H} \pm 1}, \qquad (16)$$

where m is the azimuthal quantum number. More precise details of the mode sums can be found in section 4.2.

3 Brane world black holes

3.1 Black holes in ADD brane-worlds

In the ADD brane-world scenario [17, 18, 19] space-time has $d = 4 + n$ dimensions. Our universe is a four-dimensional brane in this higher-dimensional bulk space-time. The n extra dimensions are flat and compactified (the radius of compactification is typically large compared with the Planck length but sufficiently small to agree with searches for deviations from Newton's Law of Gravitation). To avoid contradictions with precision particle-physics experiments, the forces and particles of the Standard Model are constrained to live on the brane; only gravitational degrees of freedom (gravitons and possibly scalars) can propagate in the bulk.

We model black holes in the ADD scenario in a very simple way, assuming that the brane is tensionless and infinitely thin. We also assume that the black-hole horizon is much smaller than the compactification radius of the extra dimensions. Effectively we are considering black holes in an asymptotically flat, $(4 + n)$-dimensional, space-time. Furthermore, we are particularly interested in microscopic black holes formed by the collision of particles on the brane (such a collision will not necessarily be head-on). In this case, by conservation of angular momentum, the resulting black hole will have a single axis of rotation, which will also lie in the brane.

Rotating black-hole solutions of the vacuum Einstein equations in $(4 + n)$-dimensional space-time are described by the Myers-Perry metric [25]. Unlike the situation in four space-time dimensions, the Myers-Perry metric is not unique if $n > 0$ [7, 8], and black holes need not have a spherical event-horizon topology. The general Myers-Perry metric [25] is rather lengthy, and the metrics for more complicated black objects (such as black rings) are very complex. For this reason, we restrict our attention to Myers-Perry black holes with a spherical event-horizon

topology and a single axis of rotation. In this case the general Myers-Perry metric simplifies to [25]:

$$ds^2 = -\left(1 - \frac{\mu}{\Sigma r^{n-1}}\right) dt^2 - \frac{2a\mu \sin^2 \theta}{\Sigma r^{n-1}}\, dt\, d\varphi + \frac{\Sigma}{\Delta}\, dr^2 + \Sigma\, d\theta^2$$
$$+ \left(r^2 + a^2 + \frac{a^2\mu \sin^2 \theta}{\Sigma r^{n-1}}\right) \sin^2 \theta\, d\varphi^2 + r^2 \cos^2 \theta\, d\Omega_n^2, \qquad (17)$$

where

$$\Delta = r^2 + a^2 - \frac{\mu}{r^{n-1}}, \qquad \Sigma = r^2 + a^2 \cos^2 \theta, \qquad (18)$$

and $d\Omega_n^2$ is the metric on the n-dimensional unit sphere. The mass M and angular momentum J of the black hole are given by:

$$M = \frac{1}{16\pi}\, (n+2)\, \mu\, A_{n+2}, \qquad J = \frac{2}{n+2}\, aM, \qquad (19)$$

and $A_{n+2} = 2\pi^{(n+3)/2}/\Gamma[(n+3)/2]$ is the area of the $(n+2)$-dimensional unit sphere. The horizon radius r_h of the black hole is determined through the equation $\Delta(r_h) = 0$ and it may be written as $r_h^{n+1} = \mu/(1+a_*^2)$, where $a_* = a/r_h$. When $a = 0$ and the black hole is non-rotating, the metric (17) reduces to the Schwarzschild-Tangherlini spherically-symmetric metric [57].

In (17), the co-ordinates (t, r, θ, φ) are the co-ordinates on the brane and the $d\Omega_n^2$ is the part of the metric coming from the extra dimensions. To find the metric of the higher-dimensional black hole as seen by an observer on the brane, we simply fix the co-ordinates in the extra dimensions and obtain:

$$ds^2 = -\left(1 - \frac{\mu}{\Sigma r^{n-1}}\right) dt^2 - \frac{2a\mu \sin^2 \theta}{\Sigma r^{n-1}}\, dt\, d\varphi + \frac{\Sigma}{\Delta}\, dr^2 + \Sigma\, d\theta^2$$
$$+ \left(r^2 + a^2 + \frac{a^2\mu \sin^2 \theta}{\Sigma r^{n-1}}\right) \sin^2 \theta\, d\varphi^2. \qquad (20)$$

Note that the brane metric (20) still depends on n, the number of extra dimensions. It reduces to the usual Kerr metric when $n = 0$. Although the higher-dimensional Myers-Perry metric (17) is a solution of the vacuum Einstein equations in $(4 + n)$ dimensions, the brane metric (20) is not a solution of the four-dimensional vacuum Einstein equations [58]. Instead, the space-time (20) has a non-zero classical stress-energy tensor representing an effective fluid seen by an observer on the brane. This arises from the fact that the black hole is a higher-dimensional object, but a brane observer cannot directly probe the extra dimensions [58].

3.2 Black holes in RS brane-worlds

In the RS brane-world, only one extra dimension is assumed to exist transverse to our brane. The bulk is not empty but filled with a negative cosmological constant $\Lambda_B < 0$. The higher-dimensional space-time is therefore an anti-de Sitter (AdS) space-time that contains either two (RS-I model [20]) or one (RS-II model [21]) Minkowski branes. The branes have a non-vanishing tension that, together with the bulk cosmological constant, cause the warping of the metric along the fifth dimension. In the context of the RS-I model, where two flat branes are separated in the

extra dimension by a distance a few times the Planck length, this warping is used to address the hierarchy problem. The RS-II model is by far the more interesting one from the gravitational point of view: the second brane is sent to infinity, and the warping causes the localisation of graviton close to the brane and the restoration of four-dimensional gravity despite the presence of an infinitely-extended extra dimension.

Substituting the Minkowski line-element on the brane by the Schwarzschild line-element, the following brane-world solution was found soon after in [59]:

$$ds^2 = e^{-2|y|/\ell_{AdS}} \left[- \left(1 - \frac{2M}{r} \right) dt^2 + \left(1 - \frac{2M}{r} \right)^{-1} dr^2 + r^2 \, d\Omega_2^2 \right] + dy^2 \,, \quad (21)$$

where $\ell_{AdS} = \sqrt{-6/\Lambda_B}$ is the AdS curvature length. The projection of the above five-dimensional solution on the brane, located at $y = 0$, has exactly the form of a four-dimensional black hole. However, it was demonstrated that it does not describe a regular black hole localised on the brane but rather an AdS black string that, in the context of the RS-II model, has an infinitely-extended singularity along the bulk. In addition, it suffers from a Gregory-Laflamme instability [60, 61].

Despite the numerous attempts to derive a regular, asymptotically AdS black-hole solution localised on a brane with a non-vanishing tension (for an indicative list of papers, see [62, 63, 64, 65, 66, 67, 68, 69, 70, 71, 72]; for a more complete list of references, see [30, 31, 32]), up to today no analytical solution has been constructed. Numerical studies [73, 74, 75] found black-hole solutions with horizon radius smaller than or of the order of the AdS length ℓ_{AdS} in the context of five- and six-dimensional warped models. The failure to find larger, static black-hole solutions, combined with the results following from lower-dimensional constructions of brane-world black holes [76, 77, 78], led to arguments for the non-existence of such black holes in the context of the RS model [79, 80, 81, 82, 83, 84].

A central role in this conjecture is played by the AdS/CFT correspondence: when applied in the context of the RS model [85], it dictates that classical gravity in the AdS bulk is equivalent to a strongly-coupled quantum Conformal Field Theory (CFT) living on the brane. If a five-dimensional classical solution exists, describing a regular black hole localised on the brane, then the large number of CFT modes that couple to four-dimensional gravity on the brane will cause the rapid evaporation of the black hole (we will return to this topic in section 5). Therefore, the projection of the metric on the brane ought to describe a quantum-corrected, non-static black hole; its classical counterpart in the bulk will then have to be non-static, too. This argument applies only for large-mass black holes for which the quantum corrections in the AdS bulk are negligible so that the five-dimensional solution can be considered as classical.

There are several results in the literature supporting the validity of the AdS/CFT correspondence in the RS model [30, 32], such as: the agreement in the form of the Newtonian potential on the brane, calculated through the Kaluza-Klein graviton states or the CFT brane modes, and the automatic appearance of a radiation term, that may be associated to the emission of brane CFT modes by the black hole, in the Friedmann equation on the brane. But there are also counter-arguments to the above [86, 87, 88] according to which one should not expect important quantum corrections on the brane. In support of the latter view, recent numerical studies

[89, 90, 91] find solutions that describe both small and large black holes in the context of the RS model (see also [92, 93, 94, 95, 96]).

The complexity of the bulk equations and junction conditions that one should solve to find a complete bulk/brane solution, and the non-trivial topology of the AdS space-time background are two decisive factors contributing to the difficulty in finding viable black-hole solutions in the RS model. For large-mass black holes, there might be additional, more subtle, reasons: in [70] it was shown that the brane trajectories in the background of a bulk Schwarzschild-AdS black hole are more finely-tuned for large-mass black holes; also, the recoil effect [97], that may be caused by the asymmetric emission of bulk modes resulting in the black hole leaving the brane, is more effective for large black holes than for small ones [30].

4 Hawking radiation from black holes in the ADD model

In this section we consider Hawking radiation from black holes in the ADD model, both on the brane and in the bulk. The presentation of the formalism will be based on the simply-rotating Myers-Perry black hole discussed in section 3.1 – when necessary, the spherically-symmetric limit may be recovered by setting $a = 0$. We first bring together all the relevant field equations for the different types of radiation before discussing a selection of results. The formalism for the different types of quantum field is quite involved, and here we are attempting a unified presentation. Some compromises in notation are inevitable in this situation. In particular, we always label our field modes by an index Λ, although the exact form of Λ will vary depending on the spin of the field and whether we are considering brane or bulk emission.

4.1 Formalism for field perturbations

In this subsection we consider only massless particles. The formalism outlined can be readily extended to include mass and charge. We will briefly discuss some of the effects of mass and charge on the Hawking radiation in section 4.6.

Teukolsky formalism on the brane

We now consider the formalism for massless particles of spin 0, 1/2 and 1 on the brane metric (20). Teukolsky [98, 99] developed a unified formalism for describing perturbations of a four-dimensional Kerr black hole with these spins (see also [100]). Teukolsky's original formalism also applies to spin-2 perturbations but we shall consider those separately. Teukolsky's formalism extends easily to perturbations of spin 0, 1/2 and 1 on the brane metric (20).

The Newman-Penrose formalism [101] is used to write the perturbation equations for each type of particle as a single master equation for a quantity $\Psi_s = \Psi_s(t, r, \theta, \varphi)$. The form of Ψ_s depends on the spin s of the field under consideration - details can be found in [12]. The resulting Teukolsky equation for the variable Ψ_s takes the form [55]

$$\mathcal{J}_s = \left[\frac{(r^2+a^2)^2}{\Delta} - a^2\sin^2\theta\right]\partial_t\Psi_s + \frac{2a\mu}{\Delta r^{n-1}}\partial_t\partial_\varphi\Psi_s + \left[\frac{a^2}{\Delta} - \frac{1}{\sin^2\theta}\right]\partial_\varphi\Psi_s$$
$$-\Delta^{-s}\frac{\partial}{\partial r}\left(\Delta^{s+1}\partial_r\Psi_s\right) - \frac{1}{\sin\theta}\frac{\partial}{\partial\theta}\left(\sin\theta\partial_\theta\Psi_s\right) - 2s\left[\frac{a\Delta'}{2\Delta} + \frac{i\cos\theta}{\sin^2\theta}\right]\partial_\varphi\Psi_s$$
$$+2s\left[r+\bar\rho - \frac{(r^2+a^2)\Delta'}{2\Delta}\right]\partial_t\Psi_s + s\left[s\cot^2\theta - 1 + (2-\Delta'')\delta_{s,|s|}\right]\Psi_s\,,$$
$$(22)$$

where $\bar\rho = r + ia\cos\theta$ and $\mathcal{J}_s$ is a source term, whose details for each spin s can be found in [12]. The metric function Δ is given by (18). The Teukolsky equation (22) is separable. We write

$$\Psi_s = e^{-i\omega t}e^{im\varphi}R_\Lambda(r)\,S_\Lambda(\theta), \qquad (23)$$

where $\Lambda = \{s,\omega,\ell,m\}$, ω is the field mode frequency, $m = -\ell, -\ell+1, \ldots, \ell-1, \ell$ is the azimuthal quantum number and $\ell \geq s$ is the total angular momentum quantum number. Then the following radial and angular equations are obtained [12, 55]:

$$0 = \Delta^{-s}\frac{d}{dr}\left(\Delta^{s+1}\frac{dR_\Lambda}{dr}\right) + \left[\Delta^{-1}\left(K_{\omega m}^2 - isK_{\omega m}\Delta'\right) + 4is\omega r\right.$$
$$\left.+s\delta_{s,|s|}\left(\Delta''-2\right) - a^2\omega^2 + 2ma\omega - \lambda_\Lambda\right]R_\Lambda(r), \qquad (24)$$
$$0 = \frac{1}{\sin\theta}\frac{d}{d\theta}\left(\sin\theta\frac{dS_\Lambda}{d\theta}\right) + \left[-\frac{2ms\cot\theta}{\sin\theta} - \frac{m^2}{\sin^2\theta} + a^2\omega^2\cos^2\theta - 2as\omega\cos\theta\right.$$
$$\left.+s - s^2\cot^2\theta + \lambda_\Lambda\right]S_\Lambda(\theta), \qquad (25)$$

where

$$K_{\omega m} = \left(r^2+a^2\right)\omega - am. \qquad (26)$$

The angular functions $S_\Lambda(\theta)$ are spin-weighted spheroidal harmonics [102, 103], and they and the eigenvalues λ_Λ have to be computed numerically when $a\omega \neq 0$. For $a\omega = 0$, the eigenvalues are:

$$\lambda_\Lambda = \ell(\ell+1) - s(s+1), \qquad (27)$$

and the angular functions $S_\Lambda(\theta)$ reduce to spin-weighted spherical harmonics [104].

Bulk fields

We now consider the equations satisfied by scalar and graviton perturbations of the higher-dimensional bulk metric (17).

Firstly, consider a massless scalar field propagating on the metric (17). The massless scalar wave equation is separable. We write the scalar field Ψ_0 as

$$\Psi_0 = e^{-i\omega t}e^{im\varphi}R_\Lambda(r)\,S_\Lambda(\theta)\,Y_{jn}(\Omega), \qquad (28)$$

where the index Λ is now $\{\omega,\ell,m,j,n\}$ and $Y_{jn}(\Omega)$ is a hyper-spherical harmonic [105] depending on the higher-dimensional bulk co-ordinates and indexed by an integer j. The following radial and angular equations are obtained from the scalar field equation [53]:

$$0 = \frac{1}{r^n}\frac{d}{dr}\left(r^n\Delta\frac{dR_\Lambda}{dr}\right) + \left[\Delta^{-1}K_{\omega m}^2 - a^2r^{-2}j\,(j+n-1)\right.$$
$$\left. - a^2\omega^2 + 2ma\omega - \lambda_\Lambda\right]R_\Lambda(r), \tag{29}$$

$$0 = \frac{1}{\sin\theta\cos^n\theta}\frac{d}{d\theta}\left(\sin\theta\cos^n\theta\frac{dS_\Lambda}{d\theta}\right) + \left[\omega^2a^2\cos^2\theta - \frac{m^2}{\sin^2\theta} - \frac{j\,(j+n-1)}{\cos^2\theta}\right.$$
$$\left. + \lambda_\Lambda\right]S_\Lambda(\theta). \tag{30}$$

Gravitational perturbations are much more difficult to deal with as Teukolsky's four-dimensional formalism does not readily extend to higher dimensions. A complete analysis is currently available only for higher-dimensional spherically-symmetric black holes. For spherically-symmetric black holes, a general gravitational perturbation decomposes into three parts: a symmetric traceless tensor T, a vector V and a scalar part S [106]. The master equation for each type of gravitational perturbation is separable and the relevant field quantity is written in a form similar to (28) (see [106] for details). For each type of gravitational perturbation, the radial functions satisfy the equation [107]

$$0 = \left[1 - \left(\frac{r_h}{r}\right)^{n+1}\right]\frac{d}{dr}\left\{\left[1 - \left(\frac{r_h}{r}\right)^{n+1}\right]\frac{dR_\Lambda}{dr}\right\} + \left[\omega^2 - \mathcal{V}_\Lambda\right]R_\Lambda(r), \tag{31}$$

where the form of the potential $\mathcal{V}_\Lambda$ depends on the type of gravitational perturbation. The angular functions are simply spin-weighted hyper-spherical harmonics. The index Λ now takes the form $\{B, \omega, \ell, n\}$ where $B \in \{S, V, T\}$ indicates whether we are considering a scalar (S), vector (V) or tensor (T) type of gravitational perturbation and the other labels are as before. For tensor-like and vector-like perturbations the potential $\mathcal{V}_\Lambda$ is [107]

$$\mathcal{V}_{T/V,\omega,\ell,n} = \frac{1}{r^2}\left[1 - \left(\frac{r_h}{r}\right)^{n+1}\right]\left[\ell\,(\ell+n+1) + \frac{n\,(n+2)}{4} - \frac{k}{4}\,(n+2)^2\,\frac{r_h^{n+1}}{r^{n+1}}\right], \tag{32}$$

where $k = -1$ for tensor-like (T) perturbations and $k = 3$ for vector-like (V) perturbations. For scalar-like (S) graviton perturbations, the potential has the more complicated form [107]:

$$\mathcal{V}_{S,\omega,\ell,n} = \frac{1}{r^2}\left[1 - \left(\frac{r_h}{r}\right)^{n+1}\right]\frac{qx^3 + px^2 + wx + z}{4\,[2u + (n+2)(n+3)x]^2}, \tag{33}$$

where

$$x = \frac{r_h^{n+1}}{r^{n+1}}, \qquad u = \ell\,(\ell+n+1) - n - 2, \tag{34}$$

and

$$q = (n+2)^4\,(n+3)^2,$$
$$p = (n+2)\,(n+3)\left[4u\,\left(2n^2 + 5n + 6\right) + n\,(n+2)\,(n+3)\,(n-2)\right],$$
$$w = -12u\,(n+2)\,[u\,(n-2) + n\,(n+2)\,(n+3)],$$
$$z = 16u^3 + 4u^2\,(n+2)\,(n+4). \tag{35}$$

For rotating higher-dimensional black holes, the general gravitational perturbation equations are much more complicated [108, 109, 110]. In general they are not

separable, which means that a computation of the Hawking radiation for gravitons has to date proved intractable. However, some progress can be made in the case where the higher-dimensional gravitational background is the warped product of an m-dimensional space-time $\mathcal{N}$ and an n-dimensional space $\mathcal{K}$ of constant curvature, a class of backgrounds that includes the simply-rotating Myers-Perry metric (17). In that case, the equations for tensor-type perturbations simplify considerably [111, 112] and are separable. The radial and angular equations take the forms (29–30) respectively, that is, the equations for the scalar field modes in the bulk – the only difference is that $\ell \geq 0$ for scalars and $\ell \geq 2$ for gravitons [112].

4.2 Grey-body factors and fluxes

We are interested in the fluxes of particles N, energy E and angular momentum J for the various different fields. The differential fluxes per unit time and unit frequency ω take the form:

$$\frac{d^2 N}{dt\, d\omega} = \frac{1}{2\pi} \sum_j \sum_{\ell=s}^{\infty} \sum_{m=-\ell}^{\ell} \frac{1}{e^{\tilde{\omega}/T_H} \pm 1} \mathcal{N}_\Lambda \Gamma_\Lambda, \tag{36}$$

$$\frac{d^2 E}{dt\, d\omega} = \frac{1}{2\pi} \sum_j \sum_{\ell=s}^{\infty} \sum_{m=-\ell}^{\ell} \frac{\omega}{e^{\tilde{\omega}/T_H} \pm 1} \mathcal{N}_\Lambda \Gamma_\Lambda, \tag{37}$$

$$\frac{d^2 J}{dt\, d\omega} = \frac{1}{2\pi} \sum_j \sum_{\ell=s}^{\infty} \sum_{m=-\ell}^{\ell} \frac{m}{e^{\tilde{\omega}/T_H} \pm 1} \mathcal{N}_\Lambda \Gamma_\Lambda. \tag{38}$$

Here we have written out precisely the mode sums represented schematically in (14, 16). As well as the usual sums over the angular momentum quantum numbers ℓ, m, there is an additional sum over j for scalar field emission in the bulk and tensor-type graviton emission from a rotating black hole, where j indexes the hyper-spherical harmonics in these cases. There is no sum over j for graviton emission from spherically-symmetric higher-dimensional black holes. In the thermal factor, the $+$ sign is for fermionic fields and the $-$ sign for bosonic fields. In the above, $\tilde{\omega}$ is given by (8), while the temperature T_H and angular velocity Ω_H of the simply-rotating Myers-Perry black hole (17) are found to be:

$$T_H = \frac{(n+1) + (n-1)a_*^2}{4\pi(1 + a_*^2)r_h}, \qquad \Omega_H = \frac{a}{r_h^2 + a^2}. \tag{39}$$

For each mode, the fluxes (36–38) depend on the grey-body factor Γ_Λ, and also a degeneracy factor $\mathcal{N}_\Lambda$ accounting for the multiplicity of modes having the quantum numbers $\{\omega, \ell, m, j\}$. The degeneracy factors are always independent of the mode frequency ω and azimuthal quantum number m, but depend on ℓ, j (where applicable) and the number of extra dimensions n.

On the brane, for fields of spin-1/2 and spin-1, there are field modes with two polarizations, so to take this into account we set the degeneracy factors equal to

$$\mathcal{N}_\Lambda = \begin{cases} 1 & \text{for } s = 0, \\ 2 & \text{for } s = \frac{1}{2}, \\ 2 & \text{for } s = 1. \end{cases} \tag{40}$$

For bulk scalar fields, the degeneracy factor is [53]:

$$\mathcal{N}_\Lambda = \frac{(2j + n - 1)(j + n - 2)!}{j!(n-1)!}. \tag{41}$$

For bulk graviton fields, we need to consider each type of gravitational perturbation separately. If we consider a rotating black hole, we only have separable field equations for tensor-type gravitational perturbations, in which case the degeneracy factor is [113]

$$\mathcal{N}_\Lambda = \frac{(n+1)(n-2)(n+j)(j-1)(n+2j-1)(n+j-3)!}{2(j+1)!(n-1)!}. \tag{42}$$

If, on the other hand, we consider a non-rotating black hole, all three types of gravitational perturbation (scalar S, vector V and tensor T) can be considered. The degeneracy values are then [114, 115, 116]:

$$\begin{aligned}
\mathcal{N}_{S,\omega,\ell,n} &= \frac{(2\ell + n + 1)(\ell + n)!}{(2\ell + 1)\,\ell!\,(n+1)!}, \\
\mathcal{N}_{V,\omega,\ell,n} &= \frac{\ell(\ell + n + 1)(2\ell + n + 1)(\ell + n - 1)!}{(2\ell + 1)(\ell + 1)!n!}, \\
\mathcal{N}_{T,\omega,\ell,n} &= \frac{n(n+3)(\ell + n + 2)(\ell - 1)(2\ell + n + 1)(\ell + n - 1)!}{2(2\ell + 1)(\ell + 1)!(n+1)!}.
\end{aligned} \tag{43}$$

To compute the Hawking fluxes (36–38), it remains to find the grey-body factors Γ_Λ. These are computed by numerically integrating the relevant radial equation (24, 29, 31). For an "up" mode, the grey-body factor Γ_Λ is the ratio of the flux in the mode at infinity and the flux in the out-going part of the mode near the event horizon, in other words it is the transmission coefficient for each "up" mode. The exact form of the flux depends on the spin of the field considered (see [12, 100] for details). Here we simply state the results for the grey-body factors in each case.

We first consider scalar and graviton fields, which are each described by a single radial function R_Λ which satisfies the relevant radial equation: (24) for scalar fields on the brane; (29) for scalar fields in the bulk; (31) for all types of graviton emission from a non-rotating black hole; or (29) for tensor-type graviton emission from a simply-rotating black hole. The "up" modes then have radial functions of the form:

$$R_\Lambda \sim \begin{cases} (r - r_h)^{i\tilde\omega/4\pi T_H} + C_{R,\Lambda}(r - r_h)^{-i\tilde\omega/4\pi T_H} & r \to r_h \\ C_{T,\Lambda} r^{-y} e^{i\omega r} & r \to \infty, \end{cases} \tag{44}$$

where $C_{R,\Lambda}$ and $C_{T,\Lambda}$ are complex constants, and

$$y = \begin{cases} 1 & \text{for brane emission of scalars,} \\ 1 + \frac{n}{2} & \text{for bulk emission of scalars, and tensor-type graviton emission} \\ & \text{from rotating black holes,} \\ 0 & \text{for graviton emission from non-rotating black holes.} \end{cases} \tag{45}$$

The grey-body factor is then simply

$$\Gamma_\Lambda = 1 - |C_{R,\Lambda}|^2 = \frac{\omega}{\tilde\omega} |C_{T,\Lambda}|^2. \tag{46}$$

If the black hole is non-rotating, $\tilde\omega = \omega$ and $\Gamma_\Lambda = |C_{T,\Lambda}|^2$. If the black hole is rotating, for modes with $\omega/\tilde\omega < 0$, equation (46) implies that $\Gamma_\Lambda < 0$, so we have super-radiance [100].

We next consider fermion (spin-$\frac{1}{2}$) and gauge boson (spin-1) fields, for which there are two radial functions, corresponding to $s = +|s|$ and $s = -|s|$. The radial functions R_Λ satisfy (24) and, for an "up" mode, have the asymptotic forms [12, 55]

$$R_\Lambda^{s=+|s|} \sim \begin{cases} C_{R,\Lambda} \Delta^{-s} (r - r_h)^{-i\tilde{\omega}/4\pi T_H} & r \to r_h \\ 0 & r \to \infty, \end{cases}$$

$$R_\Lambda^{s=-|s|} \sim \begin{cases} (r - r_h)^{i\tilde{\omega}/4\pi T_H} & r \to r_h \\ C_{T,\Lambda} r^{-\delta_{s,1}} e^{i\omega r} & r \to \infty, \end{cases} \tag{47}$$

for complex constants $C_{R,\Lambda}$ and $C_{T,\Lambda}$. For gauge bosons with $|s| = 1$, the grey-body factor is given by (46), and there is super-radiance for modes with $\tilde{\omega} < 0$. For fermion fields with $|s| = \frac{1}{2}$, the grey-body factor is:

$$\Gamma_\Lambda = 1 - |C_{R,\Lambda}|^2 = |C_{T,\Lambda}|^2. \tag{48}$$

For fermions, we therefore have $\Gamma_\Lambda > 0$ for all modes and no super-radiance [100].

4.3 Emission of massless fields on the brane

We now present a selection of results on the decay of higher-dimensional black holes through the emission of Hawking radiation. The presentation of the results will be by no means exhaustive, rather we hope that it will reveal some of the main features of the radiation spectra from these black holes. We will start from the emission of particles along the brane, then consider the bulk emission and finish with a discussion of the energy balance between the two decay channels.

For a brane-localised observer, the emission of particles along the brane is the only observable decay channel of a higher-dimensional black hole. Drawing information from black holes in four dimensions, we expect that higher-dimensional black holes will emit Hawking radiation during both their rotating and spherically-symmetric phase. The rotating phase is the most generic, however, it is also the most technically involved. Therefore, we will start from the spherically-symmetric phase, that, although it is chronologically second, has a significantly simpler treatment.

Non-rotating black holes

The gravitational background describing the space-time around a non-rotating, higher-dimensional black hole, i.e. the Schwarzschild-Tangerlini line-element [57], and the corresponding field equations follow easily from (20) and (24–25), respectively, by setting $a = 0$. In particular, the angular equation (25) now reduces to the one for the spin-weighted spherical harmonics with a well-defined eigenvalue, and offers no new information given the spherically-symmetric emission. Therefore, it is only the radial equation (24), significantly simplified after setting $a = 0$, that needs to be integrated. This has been performed both analytically [117, 118, 119] and numerically [120]. In the former case, an approximation technique needs to be applied: in this, the radial equation is solved in the two asymptotic regimes, i.e. near the horizon ($r \simeq r_h$) and far away from it ($r \gg r_h$), and the two solutions are matched at an intermediate point. The analytic result derived for the grey-body factor is valid only under the assumption that the energy of the emitted particle satisfies the
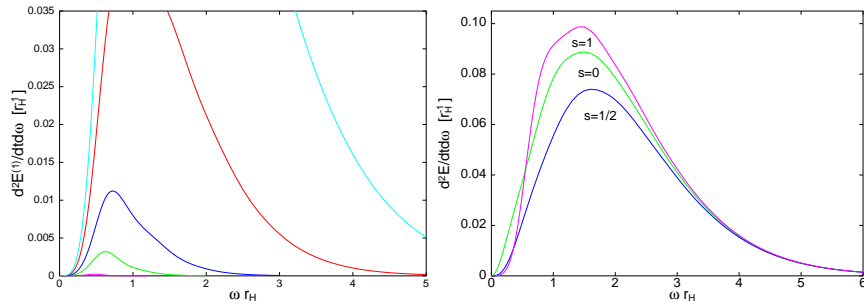
Fig. 4. Energy emission rates **(a)** for gauge bosons, for $n = 0, 1, 2, 4$ and 6 (from bottom to top) [12], and **(b)** for all species of brane-localised particles for $n = 6$ [120].

constraint $\omega r_h \ll 1$. Therefore, for the derivation of the radiation spectra beyond the low-energy regime, one needs to employ numerical methods.

In [120], the complete spectra for all types of brane particles and for arbitrary energy ω were thus numerically derived. In Figure 4(a), we depict the differential energy emission rate per unit time and unit frequency for gauge bosons emitted on the brane by a spherically-symmetric black hole, for variable n [12, 120]. We observe that, as the number of extra dimensions that are transverse to the brane increases, the black hole radiates more energy per unit time and over a much wider spectrum of frequencies. This is due to the combined effect of the grey-body factors Γ_Λ and the temperature T_H of the black hole (39), with the latter being clearly an increasing function of n, for a fixed horizon radius r_h. The same behaviour is observed for all types of brane particles, i.e. scalars, fermions and gauge bosons [12, 120]. By integrating the energy spectra over ω, we find that the total emissivities are enhanced by a factor of the order of 10^3-10^4, as n increases from 0 to 7.

The exact value of the enhancement factor, however, depends on the spin s of the particle, and that leads to the question whether the black hole prefers to emit different species of particle for different values of n. In Figure 4(b), we depict the power fluxes for particles with spin $s = 0$, $1/2$ and 1, for the case $n = 6$ [120]: the gauge bosons clearly dominate over both scalars and fermions. This result is to be compared to the four-dimensional one [4, 121, 122, 123] where scalars dominate, and to the case where n takes intermediate values, where the black hole emits almost equal amounts of energy in the three particle channels [120]. One could then propose that the emission by a higher-dimensional, spherically-symmetric black hole on the brane could reveal the number of additional spacelike dimensions [117, 118, 120].

Rotating black holes

We now turn to the preceding rotating phase that, for black holes created during a non-head-on collision, is the most generic and perhaps the only phase realised due to their short life-time. In this case, the space-time around the black hole is not spherically-symmetric – instead, the axis of rotation provides a preferred direction in space. Therefore, the angular equation, too, contains vital information about the emission process, and it is thus the set of equations (24–25) that we now need to
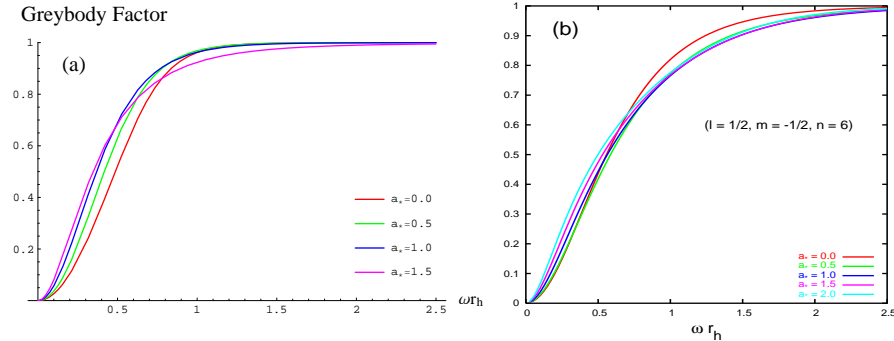
Fig. 5. Grey-body factors of brane-localised fermions derived **(a)** analytically [126] and **(b)** numerically [55] for $\ell = -m = 1/2$, $n = 6$ and variable a_*.

solve. The radial equation will provide us again with the value of the grey-body factor. For this, we need the eigenvalue λ_Λ whose value may be found by numerically integrating the angular equation. There is, however, an infinite power-series expansion [102, 103, 124], in the limit of small $a\omega$, of the form

$$\lambda_\Lambda = -s(s+1) + \sum_k f_k \left(a\omega\right)^k = \ell(\ell+1) - s(s+1) - \frac{2ms^2}{\ell(\ell+1)} a\omega + ... \quad (49)$$

The use of the above expression for λ_Λ allows for the analytical solution of the radial equation [119, 125, 126] for the rotating phase, too, and the derivation of a formula for the grey-body factor. As before, the validity of the result is limited: it applies only for emission by a slowly-rotating black hole ($a_* < 1$) in the low-energy regime ($\omega r_h \ll 1$); for the sake of comparison, in Figure 5(a,b), we present both the analytic [126] and the numerical result [55], respectively, for the grey-body factor of brane-localised fermions for the mode $\ell = -m = 1/2$ in the 10-dimensional case and for various values of a_*. The agreement between the two results is very good in the low-energy part of the spectrum and for small angular-momenta, however, it clearly worsens as either ω or a_* increases.

The complete radiation spectra, under no restrictions on the energy and angular momentum, were derived in [54, 56, 55, 127] for brane-localised scalars, fermions and gauge bosons by employing numerical techniques. In each case, the angular equation (25) was integrated first to derive the exact values of both the angular eigenvalue λ_Λ and the spin-weighted spheroidal harmonics S_Λ. The radial equation (24) was solved next from the horizon to infinity under the appropriate boundary conditions. The numerical integration of the set of radial and angular equations presents different challenges for different species of fields – we address the interested reader to [54, 56, 55, 127] for further information on how to overcome these.

For a rotating black hole, the grey-body factor depends both on the number of extra dimensions n and the angular-momentum a_* of the black hole, but also on the part of the energy spectrum and the particular mode considered. An indicative result for the grey-body factor for fermions [55] with $\ell = -m = 1/2$, $n = 6$ and various values of a_* was presented in Figure 5(b). Using the values of the numerically-derived grey-body factors, one may proceed to determine the fluxes of particles N, energy E and angular momentum J for a rotating black hole on the brane. The profile
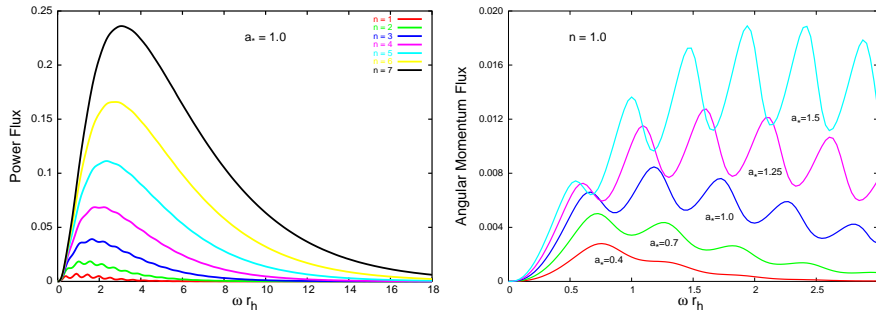
Fig. 6. (a) Energy emission rate for fermions in terms of n, for $a_* = 1$ [55], and **(b)** angular-momentum emission rate for scalars, in terms of a_*, for $n = 1$ [54].

of each flux shows an enhancement, in terms of both n and a_*, for all species of brane-localised particles. In Figure 6(a,b), we depict indicative cases of the energy emission rate for fermions, for $a_* = 1$ and various values of n [55], and of the angular-momentum emission rate for scalars, for $n = 1$ and various values of a_* [54], respectively. The enhancement factor in the total emissivity of all three fluxes, when n varies from 1 to 7, is typically of $\mathcal{O}(100)$ while the one when a_* changes from 0 to 1 is of $\mathcal{O}(10)$.

The angular equation (25) is also a source of valuable information for the emission process: the spin-weighted spheroidal harmonics $S_\Lambda(\theta)$ contain information on the angular distribution of the emitted particles. The differential fluxes (36–38) are derived by integrating the appropriate operators over a sphere at infinity. If we therefore take a step back, one may derive the differential emission rates per unit time, unit energy and unit of $\cos\theta$, where θ is the angle measured from the rotation axis of the black hole. All fluxes exhibit a non-trivial angular distribution as a result of two factors: (i) the centrifugal force, that forces all types of particles to be emitted on the equatorial plane, particularly for large values of ω or a_*, (ii) the spin-rotation coupling, which tends to align all particles with non-vanishing spin with the rotation axis – this factor has a different effect on different radiative components and is more prominent the larger the value of the spin and the smaller the energy of the particle. In Figure 7, we present three-dimensional graphs depicting the differential energy emission rate in terms of ω_* and $\cos\theta$ for scalars, fermions
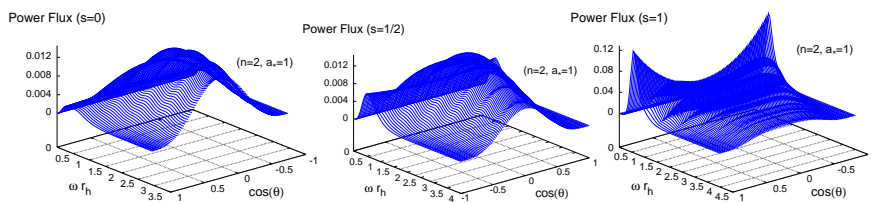

Fig. 7. Angular distribution of the power spectra for scalars [54] (left plot), fermions [55] (middle plot) and gauge bosons [56] (right plot) for $n = 2$ and $a_* = 1$.

and gauge bosons, for $n = 2$ and $a_* = 1$ [54, 55, 56], that clearly present the above behaviour. Note, that for fermions and gauge bosons, the distribution is symmetric over the two hemispheres since both radiative components, $s = \pm\frac{1}{2}$ and $s = \pm 1$, respectively, have been taken into account in the expression of the energy emission rates in each case.

The aforementioned angular distribution of the emitted particles will be a distinct observable effect, and will last for as long as the angular-momentum of the black hole is non-zero. However, for a rotating black hole, the task of drawing quantitative information from the Hawking radiation spectra, regarding the parameters of space-time, presents a serious difficulty: both the number of extra spacelike dimensions n and the angular-momentum parameter a_* cause an enhancement of the emission rates (36–38). One therefore needs to break this degeneracy, by using an observable that would depend rather strongly on the value of only one of these parameters and, at the same time, be almost insensitive to the value of the other.

As we mentioned above, one of the two factors that determine the angular distribution of the emitted particles is the spin-rotation coupling that is dominant at the low-energy regime. If we then focus on this part of the energy spectrum, and consider the emission of fermions and gauge bosons, we find the behaviour depicted in Figure 8 [128]: the gauge bosons (left plot) are aligned parallel or anti-parallel to the rotation axis of the black hole [128], while the fermions (right plot) have an angle of emission that depends on the value of the angular momentum of the black hole [128, 129]. The aforementioned pattern is in fact independent of the value n of extra dimensions. Therefore, by observing the angles of emission of gauge bosons and fermions in a low-energy channel, one could in principle determine the orientation of the rotation axis and the angular momentum, respectively, of the black hole. The diferential fluxes (36–38) could then be used to determine the value of n, too.
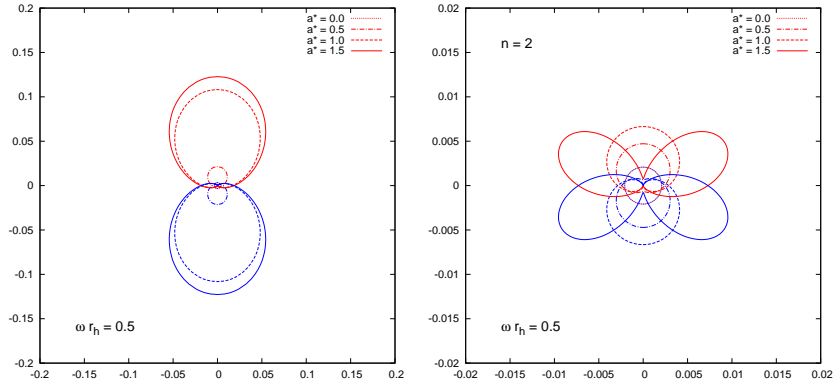
Fig. 8. Polar plots with the angular distribution of gauge bosons (left plot) and fermions (right plot) for $\omega r_h = 0.5$, $n = 6$ and variable a_* [128]. Red (upper) curves correspond to positive helicity particles and blue (lower) curves to negative helicity particles.

The results depicted in Figure 8 were found by numerically integrating both the radial and angular equations for gauge bosons and fermions. However, since the behaviour found above takes place in a low-energy channel, one could attempt to use analytic methods to solve both equations and derive the angular emission pattern. As we have already discussed, the radial equation (24) has been solved analytically for all species of brane particles [119, 125, 126]. The angular equation (25) also admits an analytic solution in the form of an infinite power-series [130]. In [131], a constraint was thus derived that semi-analytically determines the angle of maximum emission for different types of fields; the angular emission pattern of scalars, gauge bosons and fermions was then found, for a wide range of values of the angular-momentum parameter a_* and energy ω of the emitted particle.

4.4 Emission of massless fields in the bulk

Having studied the emission of Hawking radiation on the brane, i.e. the part of the emitted energy that a brane observer could potentially detect, we now turn to the emission of Hawking radiation in the bulk, i.e. the part of the emitted energy that would literally go missing. Brane observers have no access to the bulk, nevertheless, we need to study the different types of emission and estimate the amount of energy that is channeled in the bulk. Since Standard Model particles are constrained to live on the brane, the only degrees of freedom allowed to propagate in the bulk are scalars and gravitons. In what follows, we review the existing results in the literature for the corresponding radiation spectra.

We start with the emission of scalar fields: the set of equations, for the more complex rotating phase, are given in (29–30), while the ones for the spherically-symmetric phase follow by setting $a = 0$. These equations have been solved, for both phases, by employing either analytical [117, 132, 133] or numerical [53, 120, 134] methods. For the analytical approach, based on the same approximation method as in the case of brane emission, we need the angular eigenvalue λ_Λ in an analytical form: for the spherically-symmetric phase, this is known and given by [105]

$$\lambda_\Lambda = \ell(\ell + n + 1),\tag{50}$$

while for the rotating phase there is again a power-series expression [135, 136]. The analytical results thus derived for the grey-body factor may be used to describe the effect of Hawking radiation in the bulk very accurately in the low-energy regime and, at times, even in the intermediate-energy regime.

However, the complete spectra may be derived only through numerical integration. For the spherically-symmetric case, the angular equation (30) contains again no new information for the radiation process - it is only the radial equation (29), with $a = 0$, that needs to be numerically integrated. For the rotating phase, the angular equation (30) is integrated first to provide the eigenvalue λ_Λ - note that, in the absence of an observer in the bulk, there is no motivation for the study of the angular distribution of the emitted particles. The radial equation (29) is integrated next to determine the grey-body factors and, subsequently, the emitted fluxes.

We will focus on the presentation of results for the rotating phase, since the dependence on the number of extra dimensions n will become manifest when we fix the value of the angular-momentum parameter a_*. In Figure 9(a) [53], we present exact numerical results for the grey-body factor for a scalar field emitted in the bulk
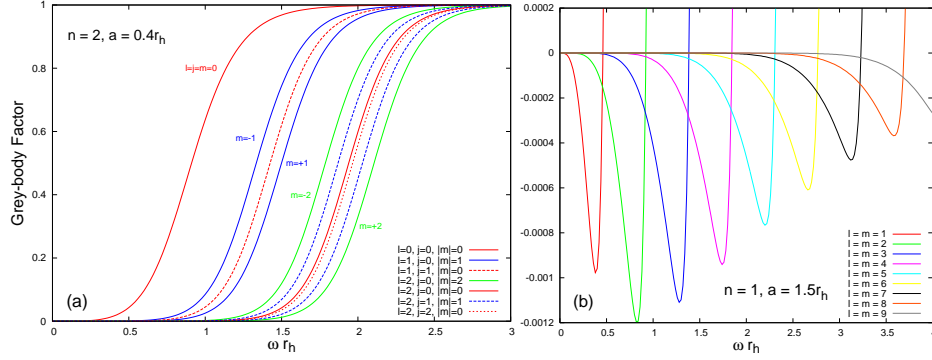
Fig. 9. Grey-body factors for a bulk scalar field: **(a)** complete results for various modes (j, ℓ, m), for $n = 2$ and $a_* = 0.4$, and **(b)** the super-radiant regime for various co-rotating modes $\ell = m$, for $n = 1$ and $a_* = 1.5$ [53].

by a six-dimensional black hole with $a_* = 0.4$: the different curves correspond to various modes characterised by the set of (j, ℓ, m) quantum numbers and show a hierarchical splitting first on ℓ, then on m and finally on j. Figure 9(b) [53] depicts the behaviour of the grey-body factor for a bulk scalar field, in the background of a black hole with $n = 1$ and $a_* = 1.5$, in the super-radiant regime, $\omega < m \, \Omega_H$: as in the case of brane emission, the super-radiance effect is most important for the maximally co-rotating modes $\ell = m$ and $j = 0$, and for low values of n.

In Figure 10(a), we depict the differential energy emission rate for bulk scalar fields [53], for fixed angular-momentum parameter $a_* = 1$, and variable n. The
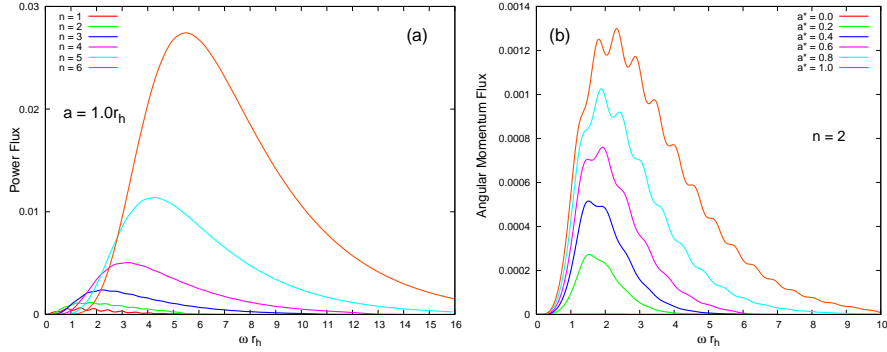
Fig. 10. **(a)** Energy emission rate for bulk scalar fields from a black hole with $a_* = 1$ and variable n, and **(b)** angular-momentum emission rate for bulk scalar fields from a black hole with $n = 2$ and variable a_* [53].
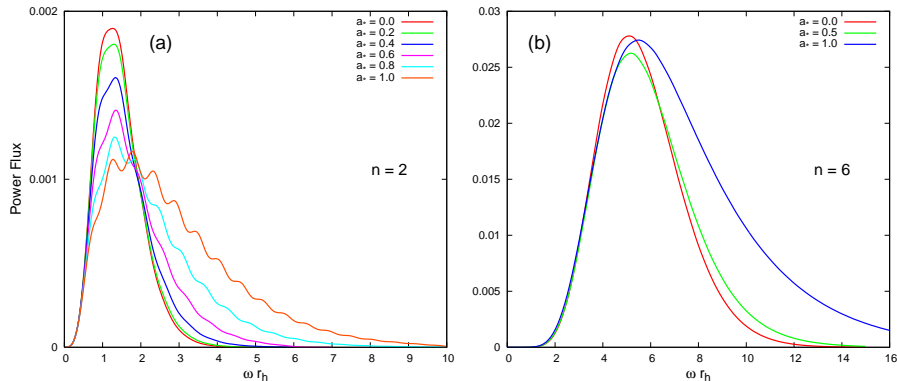
Fig. 11. Energy emission rates for scalar fields in the bulk from a black hole with **(a)** $n = 2$, and **(b)** $n = 6$, and variable a_* [53].

power flux shows a significant overall enhancement as n increases, with a small suppression at the low-energy regime and a shift of the peak of the curve towards larger energies - this behaviour is also identical to the one observed in the case of a spherically-symmetric black hole emitting scalar particles in the bulk [120]. The particle and angular-momentum fluxes were also found to have the same behaviour. The angular-momentum emission rates, presented in Figure 10(b) for $n = 2$, show a significant enhancement over the whole energy regime, as a_* increases. The power and particle fluxes, on the other hand, have a more particular profile: for low values of n, the emission curves are also shifted to the high-energy regime, as a_* increases, but their peak values are significantly suppressed, as shown in Figure 11(a); for large values of n, the energy and particle emission curves remain almost unchanged as a_* increases, apart from a small enhancement in the amount of emission at the high-energy regime; see Figure 11(b).

We now turn to the emission of gravitons in the bulk by a higher-dimensional black hole. For a spherically-symmetric black hole, the analysis is now complete. The radial equation (31), obeyed by all three types of gravitational perturbations - scalar, vector and tensor ones - has been solved analytically both in the low [114] and intermediate-energy regime [137]. The low-energy analysis [114] revealed that the graviton spectra exhibit the same behaviour as bulk scalar fields [120], i.e. a suppression at the low-energy regime and a shift of the emission curve towards higher energies, as n increased. The same analysis showed that, at the lower part of the energy spectrum, the emission of gravitons is negligible compared to that of bulk scalar fields, however that was expected to change at higher energies where higher partial modes would dominate.

That expectation was indeed proved right by the exact numerical analysis performed in [138, 139, 140]. It was thus demonstrated that the graviton radiation spectra were strongly enhanced at the higher part of the spectrum and for large values of n. The latter was largely due to the fact that the degeneracy factors of the graviton states (43) increase rapidly with both n and ℓ with the higher modes
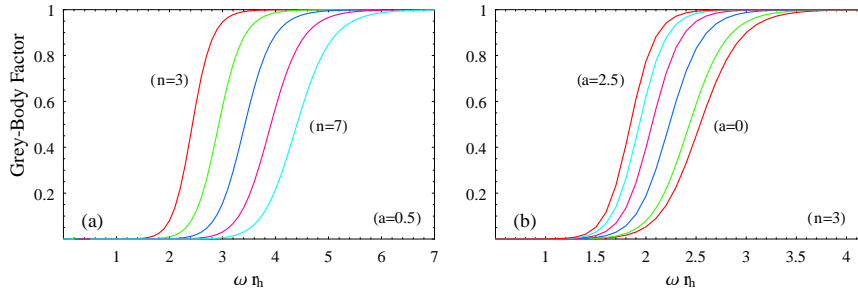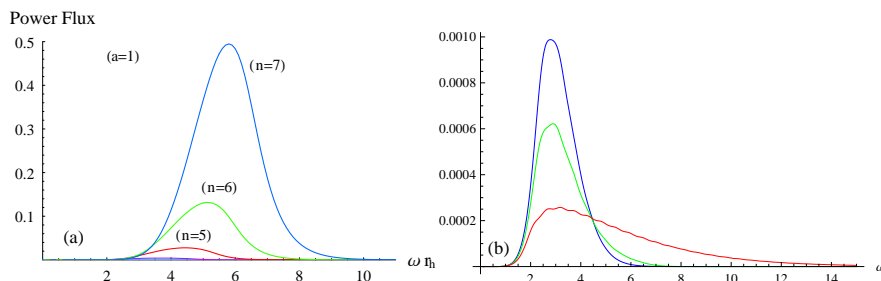
Fig. 12. Grey-body factors for tensor-type graviton modes ($\ell = j = 2, m = 0$) for:
(a) $a_* = 0.5$ and variable n, and **(b)** $n = 3$ and variable a_* [113].

dominating at the upper part of the spectrum. For example, for a moderate value of ℓ, i.e. $\ell = 5$, the number of graviton states, as n varies from 1 to 6, increases by a factor of 10^4 [114]. An interesting twist is that the tensor graviton modes, the most negligible degrees of freedom at the low-energy regime [114], proliferate as n increases. Overall, it is found [138, 139] that, as n reaches the value 7, a spherically-symmetric black hole emits 35 times more energy in the bulk in the form of gravitons than in any other particle on the brane.

For the case of the simply-rotating black hole (17), only the equations for tensor-type perturbations have been derived, and these are identical to the ones for a bulk scalar field (29–30) apart from the allowed values of the angular-momentum number l (i.e. $\ell \geq 2$ instead of $\ell \geq 0$). These equations were solved both analytically and numerically in [113], with the two sets shown to agree remarkably well even up to the intermediate-energy regime. In Fig. 12(a,b), we present exact numerical results for the grey-body factor of the lowest tensor-type mode ($\ell = j = 2, m = 0$), in terms of n and a_*, respectively [113]. We observe that, as the number of extra dimensions n increases, the grey-body factor is suppressed over the whole energy regime – a similar suppression is exhibited also by bulk scalar fields [53, 120, 133]. On the

Fig. 13. Energy emission rate for tensor-type gravitons **(a)** for $a_* = 1$ and variable n, and **(b)** for $n = 3$ and $a_* = 0, 0.5, 1.2$ (from top to bottom) [113].

other hand, the grey-body factor is strongly enhanced with the angular momentum of the black hole. Turning to the fluxes, the indicative case of the energy emission rate is presented in Figures 13(a,b) [113], in terms again of n and a_*. Similarly to the case of bulk scalars, the graviton emission rates are significantly enhanced with n, while the emission is suppressed at the low and intermediate-energy regimes and enhanced at the high-energy regime as a_* increases (for large n, the suppression at the low and intermediate-energy regimes is replaced again by a mild dependence on a_*).

4.5 Energy balance between the brane and the bulk

The question of the energy balance between the brane and bulk emission channels is an important one, not only for its theoretical interest but also for practical purposes: if we determine what fraction of the available energy of the black hole is lost in the bulk, we will know how much remains for emission on the brane, and thus how likely the observation of the Hawking radiation effect will be for the brane observer.

The study of the higher-dimensional spherically-symmetric black hole is, as we saw, now complete with the exact spectra for all types of brane and bulk particles being determined. In [53, 120], exact numerical analyses were performed in order to compare the scalar emissivity of the black hole in the brane and bulk channels. In the first row of Table 1 we display some indicative values of the proportion of the total power emitted in the bulk by a non-rotating black hole [53, 120]: we see that the bulk scalar channel is always subdominant to the brane one, but not necessarily negligible. Although bulk and brane scalar fields "see" the same black-hole temperature, their grey-body factors behave differently with n, leading to the emission of more energetic, but significantly fewer bulk scalar fields compared to the brane ones.

For the brane-localised fermions and gauge bosons and the bulk gravitons, it is again the relative behaviour of their grey-body factors, but also of their degeneracy factors, that will determine the result. Regarding the latter, we have already discussed the rapid proliferation, with n, of the gravitons in the bulk, however, the large number of Standard Model degrees of freedom living on the brane must also be taken into account. When all the above are implemented in the analysis, it is found [138, 139] that the brane channel is the most dominant during the spherically-symmetric phase of the black hole, a result that agrees with an early analytical argument [141].

The same question of the bulk-to-brane energy balance needs to be posed also for the rotating phase. The relative scalar emissivity can again be derived since the radiation spectra for bulk and brane emission are known [53, 54, 127]. The entries

Table 1. Total proportion of scalar power emitted in the bulk by a black-hole [53]

n	1	2	3	4	5	6
$a_* = 0.0$	28.3%	19.9%	17.9%	19.6%	24.8%	34.0%
$a_* = 0.5$	20.9%	13.5%	11.8%	13.0%	16.7%	24.0%
$a_* = 1.0$	12.5%	7.1%	6.2%	6.8%	9.1%	14.7%

of Table 1 reveal that, not only is the bulk scalar channel the subdominant one also during the rotating phase, but the proportion of the energy emitted in the bulk reduces with the angular-momentum of the black hole. This is due to the fact that the enhancement of the grey-body factor with a_* is not as large for bulk scalar emission as it is for the brane one.

Since we still lack the complete emission spectra for all types of gravitational perturbations in the bulk, the question of the energy balance between the brane and bulk channels for the rotating phase remains open. In [113], the total emissivity of tensor-type gravitons was compared to the one for scalar bulk emission. It was found that the energy emitted in the bulk, for small values of n, in the form of tensor modes is less than 1% of the scalar emissivity but it becomes of the order of 25%, for $n = 5$ and for the indicative value of $a_* = 1$. Recalling that the tensor modes were the dominant gravitational ones in the bulk in the case of the spherically-symmetric phase, we may conclude that, for low values of n, the brane channel wins the energy-balance contest in the rotating phase, too. Whether the same situation holds for large values of n (or larger values of a_*) will be decided only when the exact emission spectra for vector and scalar-type graviton modes are found.

4.6 Additional effects in Hawking radiation

We now discuss some further aspects of the Hawking radiation emission process. In all the studies mentioned so far, the different types of particles emitted by the black hole were assumed for simplicity to be massless. The presence of the mass, however, is expected to cause a suppression of the grey-body factors since the emission of a massive field demands more energy, and thus it is less likely to happen. The effect of the mass on the radiation spectra was studied in [58, 142, 143], for scalar fields emitted by a higher-dimensional rotating black hole, and in [144, 145], for vector fields, both transverse and longitudinal modes, on a D-dimensional Schwarzschild background. It was demonstrated that the suppression is indeed more prominent the larger the mass of the emitted field, as depicted in Figure 14(a) [142]. Although the brane channel remains the dominant one, in [142], it was shown that the presence of the mass enhances the bulk-over-brane energy ratio up to a factor of 34%.

The effect of the charge of the emitted particles was studied in [143, 145, 146]. In [146], a spherically-symmetric Reissner-Nordström black hole was considered, and it was shown that the charge of a scalar particle, similarly to its mass, causes a suppression in the bulk and brane emission spectra and enhances the bulk-to-brane emissivity. In [145], the case of a charged vector field was studied, and an inverted charge splitting effect as well as the analogue of a superradiance effect were observed in the radiation spectra. The case of a higher-dimensional rotating black hole with a brane-localised Maxwell field was considered in [143]. Although only brane emission of scalars and fermions was studied, an interesting effect was found: the radiation process exhibits a charging-up phase at the low-energy regime (where the black hole emits particles with an opposite charge compared to its own) while a phase of discharging dominates at higher energies.

In addition to particle properties, parameters that characterize the black-hole space-time background may also affect the radiation spectra and subsequently the bulk-to-brane energy balance. The cosmological constant Λ, that may be present in the part of the space-time where the black hole is formed, is one of these parameters. In [147], the radiation spectra for scalar fields emitted by a higher-dimensional
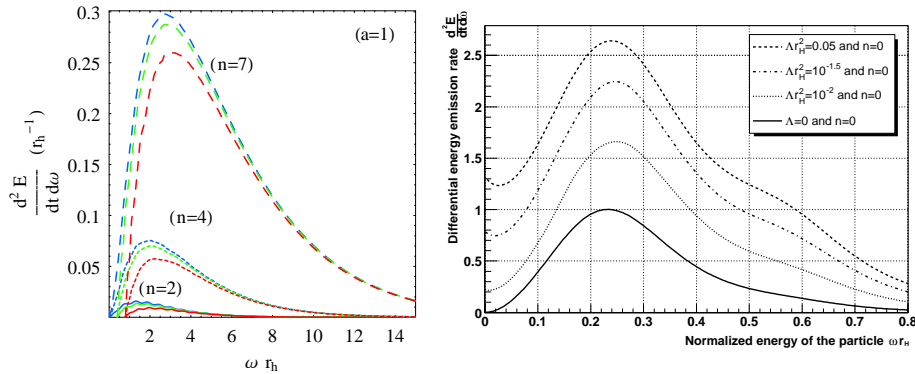
Fig. 14. Energy emission rates for scalar fields on the brane: **(a)** with $a_* = 1$, and a mass $m_\Phi = 0, 0.4, 0.8$ (from top to bottom in each set of curves) [142], and **(b)** from a Schwarzschild-de Sitter black hole with various values of Λ [147].

Schwarzschild-de Sitter black hole were studied. It was found that both bulk and brane emission rates are enhanced as the value of Λ increases, with the spectrum exhibiting a novel feature, i.e. a non-vanishing emission rate at the lowest part of the energy regime (see, Figure 14(b)). The presence of the cosmological constant was shown to increase the bulk-to-brane relative emissivity. In the case of a Kerr-de Sitter black hole [148], a similar enhancement is found when the Bousso-Hawking definition of the black hole temperature is used, whereas the use of the Hawking definition leads instead to a small decrease.

Higher-order curvature terms, such as the Gauss-Bonnet term, may be also taken into account during the decay of the black hole. Their effect on the emission spectra strongly depends on the mass of the black hole, the value of the coupling constant, and the type and energy of the emitted particle: for scalar fields, they can tilt the bulk-to-brane energy ratio in favour of the bulk [149], while, for gravitons, they can cause the suppression of their emission by many orders of magnitude leading to an increased life-time of the black hole [150]. Another counter-example of the claim that black holes radiate mainly on the brane appeared in [151] where it was shown that, in the context of a supersymmetric split-fermion model, the bulk fermion emission dominates over the brane one for $n > 1$. On the other hand, including non-commutative geometry-inspired corrections to the black hole metric significantly lowers the black hole temperature, and the bulk emission is greatly suppressed [152].

5 Hawking radiation from black holes in the RS model

Given the absence of an analytical solution describing a five-dimensional asymptotically AdS black hole localised on the brane, no exact results may be presented for the Hawking radiation process from such a black hole. Nevertheless, a number of

partial or approximate results have appeared in the literature that may shed light on some aspects of this process.

In the RS-II model, the AdS length scale ℓ_{AdS} plays the role of the effective size of the fifth dimension. On the other hand, the size of the black hole is given by the horizon radius r_h. If $r_h \ll \ell_{AdS}$, the black hole is insensitive to the warping along the fifth dimension, and it resembles a black hole in a five-dimensional flat space-time whose line-element is described by either the Myers-Perry (17) or the Tangherlini solution. In this limit, it shares all the properties of black holes in a higher-dimensional flat space-time. For example, if we assume for simplicity that the black hole is non-rotating, its horizon radius-mass relation and temperature will be given by

$$r_h = \sqrt{\frac{8}{3\pi}} \, \frac{1}{M_5} \left(\frac{M}{M_5} \right)^{1/2}, \qquad T_{BH} = \frac{1}{2\pi r_h} , \qquad (51)$$

where M and M_5 are the black-hole mass and the fundamental Planck scale, respectively. The above expressions follow readily from the corresponding $(4 + n)$-dimensional ones [153] after setting $n = 1$. Compared to a four-dimensional black hole of the same mass, for which $r_h = 2M/M_P^2$ and $T_{BH} = 1/4\pi r_h$, a small brane-world black hole has a larger horizon radius and, thus, a smaller temperature. Therefore, its evaporation rate will be significantly suppressed leading to a longer lifetime [154]

$$\frac{t_{\text{evap}}(5D)}{t_{\text{evap}}(4D)} \sim \left(\frac{\ell_{AdS}}{r_h(5D)} \right)^2 , \qquad (52)$$

the smaller the horizon radius of the five-dimensional black hole is compared to ℓ_{AdS}. The above, combined with an increased accretion rate for a brane-world black hole being formed in the early universe, radically change the mass spectrum of the primordial black holes that are expected to decay today [154, 155, 156].

As the horizon radius increases, the black hole starts to perceive the warping of the fifth dimension and its properties are correspondingly modified. Unfortunately, only numerical solutions are available in the literature in this regime. In [157], the thermodynamic properties of such a five-dimensional black-hole solution localised on the brane were studied. It was demonstrated that, for a small value of the horizon radius, the properties of the black hole match those of a five-dimensional Schwarzschild-AdS black hole. For a large value of the horizon radius, they tend to the ones of a four-dimensional Schwarzschild black hole, while in the intermediate regime they remain quite distinct from these two limits.

For $r_h \gg \ell_{AdS}$, we expect the brane-world black hole to obtain a peculiar shape: while there is no limit on its size along the brane directions, in the bulk it cannot extend at distances larger than ℓ_{AdS} due to the localisation of gravity. Thus, a large brane-world black hole has a "pancake" shape. Although it is genuinely a higher-dimensional object, it extends so little along the extra dimension and so much along the usual three that we expect it to be effectively four-dimensional and thus to resemble the Schwarzschild solution. That is, if it is allowed by the theory to exist. Even then, it is not exactly Schwarzschild.

As it was briefly mentioned in section 3.1, in reality, the projected line-element on the brane is not a vacuum solution. A four-dimensional observer would independently write the effective Einstein's equations on the brane as $G_{\mu\nu} = 8\pi G_N \, T_{\mu\nu}$. According to the AdS/CFT correspondence [85], this $T_{\mu\nu}$ is the expectation value of the stress-energy tensor operator for the CFT modes for a suitably chosen vacuum

state. The correspondence dictates that the number of CFT modes living on the brane is given by $N \sim (\ell_{AdS}/\ell_P)^2$ (where ℓ_P is the Planck length) and thus, for $\ell_{AdS} \gg \ell_P$, this number is expected to be very large. In [82], it was then argued that the presence of such a large number of fields in the vicinity of the black hole will greatly enhance its evaporation rate resulting in a large-mass black hole having a life-time given by [84]

$$t_{\mathrm{evap}} = 116 \times \left(\frac{1\,\mathrm{mm}}{\ell_{AdS}}\right)^2 \left(\frac{M}{M_\odot}\right)^3 \mathrm{years}\,. \tag{53}$$

For such a rapidly evaporating black hole, no static solution can be found to describe it even approximately. Since the line-element on the brane is merely the projection of the five-dimensional one, the bulk solution could not be static either, but rather must describe an evaporating black hole on the brane while remaining classical. In [82], a "classical evaporation" process was proposed: instabilities of the solution along the bulk cause the deformation of the horizon radius and its elongation towards the AdS boundary; for its total horizon area to remain constant, the area of the intersection of the black hole with the brane will have to decrease, and that will be viewed by a four-dimensional observer as an evaporation process.

The authors of [86] counter-argued that the above scenario assumes the involvement of all CFT brane modes in the evaporation process. But if the CFT on the brane is strongly-coupled, as the AdS/CFT correspondence dictates, would all modes be available to interact with the four-dimensional black hole? Most likely not, therefore one should not expect important quantum corrections to the four-dimensional line-element. In support of this, in [87] a Schwarzschild-AdS$_4$ black string, proven to be stable, was considered and the question was asked: why is this five-dimensional classical solution quantum-corrected on the brane (the same question for the black string of [59] loses part of its validity due to its instability)? The stress-energy tensor for the boundary field theory was computed and shown to lead to a mere renormalization of the effective cosmological constant, and not to a radiation term. In addition, in [88] it was recently suggested that a low-energy theory, such as the CFT theory on the brane, needs to be carefully UV-completed before predictions for the IR behaviour of the theory are made. When this is properly done, it follows that the emission of CFT modes in the RS-II model is significantly suppressed - in fact, it was argued that, at distances $L \leq N\,\ell_P$, low-energy CFT does not even exist.

The numerical nature of the solutions found in [89, 90, 91], describing both small and large black holes in the RS-II model, does not allow us to analytically study the effect that the brane tension or the bulk cosmological constant have on the evaporation process. In the context of a six-dimensional model, a solution was found [158] that described a black hole localised on a codimension-two brane with tension. The solution was asymptotically flat, and not AdS as in the RS-II model, and it had a peculiar horizon radius-mass relation: the closer the brane tension to the fundamental scale M_6, the larger the horizon radius is. It was shown [159] that an increase in the brane tension simultaneously decreases the black-hole temperature and increases the potential barrier, thus causing the suppression of both bulk and brane emission rates.

6 Conclusions

In this chapter we have reviewed some key aspects of our understanding of Hawking radiation from higher-dimensional black holes. One motivation for this study, apart from its intrinsic theoretical interest, is the exciting possibility of observing Hawking radiation from microscopic higher-dimensional black holes produced in high-energy collisions at either the LHC or in cosmic rays.

We began with a discussion of the quantum-field-theoretic foundations of Hawking radiation, from its original derivation for a quantum field on a dynamical space-time representing a black hole formed by gravitational collapse, to its modelling using the Unruh state on an eternal black hole geometry. After a brief review of classical black hole geometries in both the ADD and RS brane-worlds, most of this chapter has been devoted to the Hawking emission from these black holes.

For black holes in the ADD brane-world, for which we have an exact space-time metric, we gave an overview of the formalism used to describe the emission of massless particles both on the brane and in the bulk. We then reviewed a selection of results on the nature of the emission, including the important question of how much Hawking radiation escapes into the bulk and is therefore inaccessible to a brane-localised observer. Except for the emission of scalar- and vector-like graviton modes from a rotating black hole, our understanding of the emission of massless particles is essentially complete. We also briefly summarized some features of the Hawking radiation when other effects, such as the mass and charge of the emitted particles or a cosmological constant, are included.

In the RS brane-world, the lack of an exact classical metric for a black hole localized on the brane implies a scarcity of precise results on the nature of the Hawking emission from such black holes. We have therefore just briefly outlined some of the work in the literature in this case.

Our review has revealed that Hawking radiation from higher-dimensional black holes is more complicated than from four-dimensional black holes, with many features depending on the number of extra dimensions and the angular momentum of the black hole. Many of the results we have outlined in this chapter have been incorporated into simulations of black hole events at the LHC [22, 23]. Hawking radiation from black holes at the LHC characteristically involves large numbers of energetic particles, the details of the distribution and nature of the particles depending on the number of extra dimensions, the mass of the black hole and its angular momentum. Searches for these types of events have been made at the LHC, with no evidence to date for black holes [160, 161, 162, 163, 164, 165]. This non-observation of black hole events sets lower bounds on the energy scale of quantum gravity. With the LHC planned to run at higher energies and searches for high-energy black hole events in cosmic rays, accurate modelling of Hawking radiation from higher-dimensional black holes continues to be essential for experimental probes of quantum gravity.

References

1. S. W. Hawking, Commun. Math. Phys. **43**, 199–220 (1975)
2. S. Hossenfelder and L. Smolin, Phys. Rev. D **81**, 064009 (2010)
3. S. D. Mathur, Class. Quant. Grav. **26**, 224001 (2009)
4. D. N. Page, Phys. Rev. D **13**, 198–206 (1976)
5. D. N. Page, Phys. Rev. D **14**, 3260–3273 (1976)
6. D. N. Page, Phys. Rev. D **16**, 2402–2411 (1977)
7. R. Emparan and H. S. Reall, Living Rev. Rel. **11**, 6 (2008)
8. S. Tomizawa and H. Ishihara, Prog. Theor. Phys. Suppl. **189**, 7–51 (2011)
9. T. Banks and W. Fischler, `hep-th/9906038` (1999)
10. S. Dimopoulos and G. L. Landsberg, Phys. Rev. Lett. **87**, 161602 (2001)
11. S. B. Giddings and S. D. Thomas, Phys. Rev. D **65**, 056010 (2002)
12. P. Kanti, Int. J. Mod. Phys. A **19**, 4899–4951 (2004)
13. G. L. Landsberg, Eur. Phys. J. C **33**, S927–S931 (2004)
14. A. S. Majumdar and N. Mukherjee, Int. J. Mod. Phys. D **14**, 1095–1129 (2005)
15. S. C. Park, Prog. Part. Nucl. Phys. **67**, 617–650 (2012)
16. B. Webber, `hep-ph/0511128` (2005)
17. N. Arkani-Hamed, S. Dimopoulos and G. R. Dvali, Phys. Lett. B **429**, 263–272 (1998)
18. I. Antoniadis, N. Arkani-Hamed, S. Dimopoulos and G. R. Dvali, Phys. Lett. B **436**, 257–263 (1998)
19. N. Arkani-Hamed, S. Dimopoulos and G. R. Dvali, Phys. Rev. D **59**, 086004 (1999)
20. L. Randall and R. Sundrum, Phys. Rev. Lett. **83**, 3370–3373 (1999)
21. L. Randall and R. Sundrum, Phys. Rev. Lett. **83**, 4690–4693 (1999)
22. D.-C. Dai, G. Starkman, D. Stojkovic, C. Issever, E. Rizvi and J. Tseng, Phys. Rev. D **77**, 076007 (2008)
23. J. A. Frost, J. R. Gaunt, M. O. P. Sampaio, M. Casals, S. R. Dolan, M. A. Parker and B. R. Webber, JHEP **0910**, 014 (2009)
24. W. G. Unruh, Phys. Rev. D **14**, 870–892 (1976)
25. R. C. Myers and M. J. Perry, Annals Phys. **172**, 304–347 (1986)
26. A. Casanova and E. Spallucci, Class. Quant. Grav. **23**, R45–R62 (2006)
27. P. Kanti, Lect. Notes Phys. **769**, 387–423 (2009)
28. P. Kanti, Rom. J. Phys. **57**, 879–893 (2012)
29. E. Winstanley, `arXiv:0708.2656 [hep-th]` (2007)
30. R. Gregory, Lect. Notes Phys. **769**, 259–298 (2009)
31. P. Kanti, J. Phys. Conf. Ser. **189**, 012020 (2009)
32. N. Tanahashi and T. Tanaka, Prog. Theor. Phys. Suppl. **189**, 227–268 (2011)
33. J. B. Hartle and S. W. Hawking, Phys. Rev. D **13**, 2188–2203 (1976)
34. T. Damour and R. Ruffini, Phys. Rev. D **14**, 332–334 (1976)
35. U. H. Gerlach, Phys. Rev. D **14**, 1479–1508 (1976)
36. R. Parentani and R. Brout, Int. J. Mod. Phys. D **1**, 169–191 (1992)

37. R. Brout, S. Massar, R. Parentani and P. Spindel, Phys. Rept. **260**, 329–454 (1995)
38. B. L. Hu and A. Raval, Mod. Phys. Lett. A **11**, 2625–2638 (1996)
39. S. Massar and R. Parentani, Nucl. Phys. B **575**, 333–356 (2000)
40. M. K. Parikh and F. Wilczek, Phys. Rev. Lett. **85**, 5042–5045 (2000)
41. R. Schutzhold, Phys. Rev. D **64**, 024029 (2001)
42. S. Shankaranarayanan, T. Padmanabhan and K. Srinivasan, Class. Quant. Grav. **19**, 2671–2688 (2002)
43. M. Visser, Int. J. Mod. Phys. D **12**, 649–661 (2003)
44. A. Peltola, Class. Quant. Grav. **26**, 035014 (2009)
45. A. C. Ottewill and E. Winstanley, Phys. Rev. D **62**, 084018 (2000)
46. M. Casals, S. R. Dolan, B. C. Nolan, A. C. Ottewill and E. Winstanley, Phys. Rev. D **87**, 064027 (2013)
47. M. Casals and A. C. Ottewill, Phys. Rev. D **71**, 124016 (2005)
48. S. M. Christensen, Phys. Rev. D **14**, 2490–2501 (1976)
49. S. M. Christensen, Phys. Rev. D **17**, 946–963 (1978)
50. Y. Decanini and A. Folacci, Phys. Rev. D **78**, 044025 (2008)
51. V. P. Frolov and K. S. Thorne, Phys. Rev. D **39**, 2125–2154 (1989)
52. J. L. Synge, Relativity: the general theory. North-Holland, Amsterdam (1960)
53. M. Casals, S. R. Dolan, P. Kanti and E. Winstanley, JHEP **0806**, 071 (2008)
54. G. Duffy, C. Harris, P. Kanti and E. Winstanley, JHEP **0509**, 049 (2005)
55. M. Casals, S. R. Dolan, P. Kanti and E. Winstanley, JHEP **0703**, 019 (2007)
56. M. Casals, P. Kanti and E. Winstanley, JHEP **0602**, 051 (2006)
57. F. R. Tangherlini, Nuovo Cim. **27**, 636–651 (1963)
58. M. O. P. Sampaio, JHEP **0910**, 008 (2009)
59. A. Chamblin, S. W. Hawking and H. S. Reall, Phys. Rev. D **61**, 065007 (2000)
60. R. Gregory and R. Laflamme, Phys. Rev. Lett. **70**, 2837–2840 (1993)
61. R. Gregory, Class. Quant. Grav. **17**, L125–L132 (2000)
62. N. Dadhich, R. Maartens, P. Papadopoulos and V. Rezania, Phys. Lett. B **487**, 1–6 (2000)
63. G. Kofinas, E. Papantonopoulos and V. Zamarias, Phys. Rev. D **66**, 104028 (2000)
64. P. Kanti and K. Tamvakis, Phys. Rev. D **65**, 084010 (2002)
65. P. Kanti, I. Olasagasti and K. Tamvakis, Phys. Rev. D **68**, 124001 (2003)
66. R. Casadio, A. Fabbri and L. Mazzacurati, Phys. Rev. D **65**, 084040 (2002)
67. V. P. Frolov, M. Snajdr and D. Stojkovic, Phys. Rev. D **68**, 044002 (2003)
68. D. Karasik, C. Sahabandu, P. Suranyi and L. C. R. Wijewardhana, Phys. Rev. D **70**, 064007 (2004)
69. C. Galfard, C. Germani and A. Ishibashi, Phys. Rev. D **73**, 064014 (2006)
70. S. Creek, R. Gregory, P. Kanti and B. Mistry, Class. Quant. Grav. **23**, 6633–6658 (2006)
71. R. Casadio and J. Ovalle, Phys. Lett. B **715**, 251–255 (2012)
72. P. Kanti, N. Pappas and K. Zuleta, Class. Quant. Grav. **30**, 235017 (2013)
73. H. Kudoh, T. Tanaka and T. Nakamura, Phys. Rev. D **68**, 024035 (2002)
74. H. Kudoh, Phys. Rev. D **69**, 104019 (2004) [Erratum-ibid. D **70**, 029901 (2004)]
75. N. Tanahashi and T. Tanaka, JHEP **0803**, 041 (2008)
76. R. Emparan, G. T. Horowitz and R. C. Myers, JHEP **0001**, 007 (2000)
77. R. Emparan, G. T. Horowitz and R. C. Myers, JHEP **0001**, 021 (2000)
78. M. Anber and L. Sorbo, JHEP **0807**, 098 (2008)

79. M. Bruni, C. Germani and R. Maartens, Phys. Rev. Lett. **87**, 231302 (2001)
80. M. Govender and N. Dadhich, Phys. Lett. B **538**, 233–238 (2002)
81. G. Kofinas and E. Papantonopoulos, JCAP **0412**, 011 (2004)
82. T. Tanaka, Prog. Theor. Phys. Suppl. **148**, 307–316 (2003)
83. R. Emparan, A. Fabbri and N. Kaloper, JHEP **0208**, 043 (2002)
84. R. Emparan, J. Garcia-Bellido and N. Kaloper, JHEP **0301**, 079 (2003)
85. S. W. Hawking, T. Hertog and H. S. Reall, Phys. Rev. D **62**, 043501 (2000)
86. A. L. Fitzpatrick, L. Randall and T. Wiseman, JHEP **0611**, 033 (2006)
87. R. Gregory, S. F. Ross and R. Zegers, JHEP **0809**, 029 (2008)
88. N. Kaloper, Phys. Rev. D **86**, 104052 (2012)
89. P. Figueras and T. Wiseman, Phys. Rev. Lett. **107**, 081101 (2011)
90. S. Abdolrahimi, C. Cattoen, D. N. Page and S. Yaghoobpour-Tari, Phys. Lett. B **720**, 405–409 (2013)
91. S. Abdolrahimi, C. Cattoen, D. N. Page and S. Yaghoobpour-Tari, JCAP **1306**, 039 (2013)
92. M. Heydari-Fard and H. R. Sepangi, JCAP **0902**, 029 (2009)
93. D.-C. Dai and D. Stojkovic, Phys. Lett. B **704**, 354–359 (2011)
94. H. Yoshino, JHEP **0901**, 068 (2009)
95. B. Kleihaus, J. Kunz, E. Radu and D. Senkbeil, Phys. Rev. D **83**, 104050 (2011)
96. B. Cuadros-Melgar, E. Papantonopoulos, M. Tsoukalas and V. Zamarias, Phys. Rev. Lett. **100**, 221601 (2008)
97. V. P. Frolov and D. Stojkovic, Phys. Rev. D **66**, 084002 (2002)
98. S. A. Teukolsky, Phys. Rev. Lett. **29**, 1114–1118 (1972)
99. S. A. Teukolsky, Astrophys. J. **185**, 635–647 (1973)
100. S. Chandrasekhar, The mathematical theory of black holes. Oxford University Press (1998)
101. E. Newman and R. Penrose, J. Math. Phys. **3**, 566–578 (1962)
102. E. D. Fackerell and R. G. Crossman, J. Math. Phys. **18**, 1849–1854 (1977)
103. E. Seidel, Class. Quant. Grav. **6**, 1057–1062 (1989)
104. J. N. Goldberg, A. J. MacFarlane, E. T. Newman, F. Rohrlich and E. C. G. Sudarshan, J. Math. Phys. **8**, 2155–2161 (1967)
105. C. Muller, Spherical harmonics. Springer-Verlag (1966)
106. H. Kodama and A. Ishibashi, Prog. Theor. Phys. **110**, 701–722 (2003)
107. A. Ishibashi and H. Kodama, Prog. Theor. Phys. **110**, 901–919 (2003)
108. M. Durkee and H. S. Reall, Phys. Rev. D **83**, 104044 (2011)
109. H. S. Reall, Int. J. Mod. Phys. D **21**, 1230001 (2012)
110. K. Murata, Prog. Theor. Phys. Suppl. **189**, 210–226 (2011)
111. H. Kodama, Prog. Theor. Phys. Suppl. **172**, 11–20 (2008)
112. H. Kodama, Lect. Notes Phys. **769**, 427–470 (2009)
113. P. Kanti, H. Kodama, R. A. Konoplya, N. Pappas and A. Zhidenko, Phys. Rev. D **80**, 084016 (2009)
114. S. Creek, O. Efthimiou, P. Kanti and K. Tamvakis, Phys. Lett. B **635**, 39–49 (2006)
115. M. A. Rubin and C. R. Ordonez, J. Math. Phys. **25**, 2888–2894 (1984)
116. M. A. Rubin and C. R. Ordonez, J. Math. Phys. **26**, 65–67 (1985)
117. P. Kanti and J. March-Russell, Phys. Rev. D **66**, 024023 (2002)
118. P. Kanti and J. March-Russell, Phys. Rev. D **67**, 104019 (2003)
119. D. Ida, K. Y. Oda and S. C. Park, Phys. Rev. D **67**, 064025 (2003) [Erratum-ibid. D **69**, 049901 (2004)]

120. C. M. Harris and P. Kanti, JHEP **0310**, 014 (2003)
121. N. Sanchez, Phys. Rev. D **16**, 937–945 (1977)
122. N. Sanchez, Phys. Rev. D **18**, 1030–1036 (1978)
123. N. Sanchez, Phys. Rev. D **18**, 1798–1804 (1978)
124. A. A. Starobinskii and S. M. Churilov, Sov. Phys. JETP **38**, 1–5 (1974)
125. S. Creek, O. Efthimiou, P. Kanti and K. Tamvakis, Phys. Rev. D **75**, 084043 (2007)
126. S. Creek, O. Efthimiou, P. Kanti and K. Tamvakis, Phys. Rev. D **76**, 104013 (2007)
127. C. M. Harris and P. Kanti, Phys. Lett. B **633**, 106–110 (2006)
128. M. Casals, S. R. Dolan, P. Kanti and E. Winstanley, Phys. Lett. B **680**, 365–370 (2009)
129. A. Flachi, M. Sasaki and T. Tanaka, JHEP **0905**, 031 (2009)
130. E. W. Leaver, Proc. Roy. Soc. London A **402**, 285–298 (1985)
131. P. Kanti and N. Pappas, JHEP **1212**, 019 (2012)
132. V. Frolov and D. Stojkovic, Phys. Rev. D **67**, 084004 (2003)
133. S. Creek, O. Efthimiou, P. Kanti and K. Tamvakis, Phys. Lett. B **656**, 102–111 (2007)
134. E. Jung and D. K. Park, Nucl. Phys. B **731** 171–187 (2005)
135. E. Berti, V. Cardoso and M. Casals, Phys. Rev. D **73** 024013 (2006) [Erratum-ibid. D **73** 109902 (2006)]
136. V. Cardoso, G. Siopsis and S. Yoshida, Phys. Rev. D **71**, 024019 (2005)
137. A. S. Cornell, W. Naylor and M. Sasaki, JHEP **0602**, 012 (2006)
138. V. Cardoso, M. Cavaglia and L. Gualtieri, Phys. Rev. Lett. **96**, 071301 (2006) [Erratum-ibid. **96**, 219902 (2006)]
139. V. Cardoso, M. Cavaglia and L. Gualtieri, JHEP **0602**, 021 (2006)
140. D. K. Park, Phys. Lett. B **638**, 246–252 (2006)
141. R. Emparan, G. T. Horowitz and R. C. Myers, Phys. Rev. Lett. **85**, 499–502 (2000)
142. P. Kanti and N. Pappas, Phys. Rev. D **82**, 024039 (2010)
143. M. O. P. Sampaio, JHEP **1002**, 042 (2010)
144. C. Herdeiro, M. O. P. Sampaio and M. Wang, Phys. Rev. D **85**, 024005 (2012)
145. M. Wang, M. O. P. Sampaio and C. Herdeiro, Phys. Rev. D **87**, 044011 (2013)
146. E. Jung and D. K. Park, Nucl. Phys. B **717**, 272–303 (2005)
147. P. Kanti, J. Grain and A. Barrau, Phys. Rev. D **71**, 104002 (2005)
148. J. Doukas, H. T. Cho, A. S. Cornell and W. Naylor, Phys. Rev. D **80**, 045021 (2009)
149. J. Grain, A. Barrau and P. Kanti, Phys. Rev. D **72**, 104016 (2005)
150. R. A. Konoplya and A. Zhidenko, Phys. Rev. D **82**, 084003 (2010)
151. H. T. Cho, A. S. Cornell, J. Doukas and W. Naylor, Phys. Rev. D **77**, 016004 (2008)
152. P. Nicolini and E. Winstanley, JHEP **1111**, 075 (2011)
153. P. C. Argyres, S. Dimopoulos and J. March-Russell, Phys. Lett. B **441**, 96–104 (1998)
154. R. Guedens, D. Clancy and A. R. Liddle, Phys. Rev. D **66**, 043513 (2002)
155. A. S. Majumdar, Phys. Rev. Lett. **90**, 031303 (2003)
156. Y. Sendouda, S. Nagataki and K. Sato, Phys. Rev. D **68**, 103510 (2003)
157. H. Kudoh, Prog. Theor. Phys. **110**, 1059–1069 (2004)
158. N. Kaloper and D. Kiley, JHEP **0603**, 077 (2006)

159. D. C. Dai, N. Kaloper, G. D. Starkman and D. Stojkovic, Phys. Rev. D **75**, 024043 (2007)
160. G. Aad *et al.* [ATLAS Collaboration], Phys. Lett. B **709**, 322–340 (2012)
161. G. Aad *et al.* [ATLAS Collaboration], Phys. Lett. B **716**, 122–141 (2012)
162. G. Aad *et al.* [ATLAS Collaboration], Phys. Rev. D **88**, 072001 (2013)
163. V. Khachatryan *et al.* [CMS Collaboration], Phys. Lett. B **697**, 434–453 (2011)
164. S. Chatrchyan *et al.* [CMS Collaboration], JHEP **1204**, 061 (2012)
165. S. Chatrchyan *et al.* [CMS Collaboration], JHEP **1307**, 178 (2013)